UCLouvain

AGRO LOUVAIN

Faculté des bioingénieurs

Evaluation of the impacts of climate change on the distribution of Florida stone crab larvae on the West Florida Shelf

Author: Lauranne Alaerts
Promotor: Prof. Emmanuel Hanert
Readers: Prof. Philip Gravinese
Prof. Pierre Defourny
Academic year 2020-2021
Thesis presented in partial fulfillment of the requirements for the degree of Master in Bioengineering: Environmental sciences and technologies

Abstract

Ocean acidification and ocean warming are the two components of climate change that impacts marine life the most. The commercially important Florida stone crab, *Menippe mercenaria*, is one of the species that is going to be affected by those changes. In this study we investigated the impacts of climate change on the distribution of the stone crab larvae on the West Florida Shelf. To understand the dispersion of the larvae, we coupled SLIM3D, a multi-scale ocean model, with a larval dispersal model. We then conducted a connectivity study and evaluated the impacts of climate change analyzing three different scenarios, one presenting the dispersion of the larvae for present conditions and the two others presenting the dispersion for mild and extreme climate change. The results show a clear impact of climate change on larval dispersal and on the subsequent crabs distribution. In the future, climate change could result in stone crabs moving north or to deeper waters. The second impact would be the increase in the number of larvae settling in the non-fishing zone, where the water depth exceeds 30 m. The distance traveled by larvae is going to decrease, resulting in an increase of self-recruitment and decrease of the size of sub-populations. The last impact we identified is the possibility of a shift of the spawning period earlier in the season. We also evaluated that the habitats in the non-fishing zone cannot serve as a significant source of larvae for the habitats in the fishing zone since there is very little exchange between the two zones. Overall, this work could help local authorities to better understand *M. mercenaria* and to take actions regarding the fishery management and its future considering the upcoming changes in the ocean conditions.

Acknowledgements

At the end of this thesis, there are many people that I wish to thank.

First of all, I'm extremely grateful to my supervisor, Emmanuel Hanert, for being such an excellent thesis supervisor. His continuous support and enthusiasm kept me motivated throughout the year. The many meetings we had allowed me to stay focused and to constantly want to improve my work. Thanks should also go to Daniel Holstein for the opportunity to work on this subject.

I would also like to thank Thomas Dobbelaere, for always coming to the rescue every time we had a problem with SLIM. I also thank the rest of the SLIM team for their help and positive feedback on my presentation.

A special thanks goes to my fellow master students, Constance, Riana and Thomas. I especially thank Constance and Riana for the mutual support through the many bugs and problems encountered during this work. I wish them all good luck with the writing and oral presentation.

I also thank Philip Gravinese and Pierre Defourny for accepting to be the readers of this thesis. A special mention goes to Philip Gravinese, for sharing his data with me and answering my questions on the stone crab.

Finally, I would like to thank my friends and family, who helped me to hold on through this difficult year. A special thanks to my mom, for proofreading this work even if this thesis is far from her area of expertise, and to Aymeric, Maud, Nadia, Savannah and Sophie for the numerous Teams meeting, both the studious and relaxing ones.

Contents

List of variables and parameters

Symbol	Description	Units
C_D	Drag coefficient	-
C_{ij}	Connectivity between source habitat *i* and sink habitat *j*	Number of particles
$\tilde{C}_{ij}$	Normalized connectivity between source habitat *i* and sink habitat *j*	-
$\mathrm{d_{ij}}$	Distance between habitats *i* and *j*	km
$\boldsymbol{e}_z$	Vertical unit vector	-
f	Coriolis factor	1/s
g	Earth's gravitational acceleration	m/s^2
h	Water depth	m
H	Total height of the water column	m
$\boldsymbol{K}$	Diffusivity tensor	m^2/s
LS_j	Proportion of larvae that settle on habitat *j* compared to the total number of larvae released	-
$\mathrm{n_{ji}}$	Number of habitats *j* to which habitat *i* sends larvae	Number of habitats
p	Hydrostatic pressure	Pa
p_a	Atmospheric pressure	N/m2
S	Salinity	g/kg
S_i	Number of particles seeded by habitat *i*	Number of particles
$\mathrm{SI_i}$	Source index of habitat *i*	Number of habitats
SR_j	Self-recruitment index	-
T	Temperature	°C
t_m	Time since midnight	s
$\mathrm{t_{relax}}$	Relaxation time	days
$\boldsymbol{u}$	Horizontal velocity	m/s
$\boldsymbol{u}_L$	Total velocity of the larva	m/s
v	Vertical eddy viscosity	m^2/s
v_h	Horizontal eddy viscosity	m^2/s
w	Vertical velocity	m/s
w_L	Vertical velocity of the larva	m/s
$\mathrm{w_B}$	Biological component of the vertical velocity of the larvae	m/s
$\mathrm{w_{d,i}}$	Downward swimming velocity of larval stage *i*	m/s
$\mathrm{w_{d,M}}$	Downward swimming velocity of megalopal stage	m/s
$\mathrm{w_{u,i}}$	Upward swimming velocity of larval stage *i*	m/s
$\mathrm{w_{Li}}$	Vertical velocity of the larvae in response to light	m/s
$\mathrm{w_{pH}}$	Vertical velocity of the larvae in response to pH	m/s
w_W	Vertical velocity of the water	m/s
$\mathrm{WCL_i}$	Weighted connectivity length of habitat *i*	km
$\boldsymbol{X}$	Position of the larva	m
z_r	Surface layer thickness	m
z_0	Friction length	m

$\alpha_{p,i}$	Correction factor for the vertical velocity of the larva in response to pressure	-
η	Sea surface elevation	m
κ	Vertical eddy diffusivity	m^2/s
κ_h	Horizontal eddy diffusivity	m^2/s
κ_K	von Kármán constant	-
$\kappa_{\boldsymbol{L,h}}$	Horizontal diffusivity of the larva	m^2/s
κ_L	Vertical diffusivity of the larva	m^2/s
ρ	Ocean water density	kg/m^3
ρ_0	Reference density	kg/m^3
τ_b	Bottom friction stress	N/m^2
τ_s	Surface wind stress	N/m^2
φ	Latitude	°
Ω	Earth rotation's speed	radians/s
$d\boldsymbol{W}(t)$	Wiener noise increment	-
$\boldsymbol{\nabla}_h$	Horizontal gradient operator	-
$//$	Floor division operator	-
$\%$	Modulo operator	-

List of acronyms

CM: Connectivity matrix

GOM: Gulf of Mexico

HYCOM: HYbrid Coordinate Ocean Model

LPT: Lagrangian particle tracker

NOAA: National Oceanic and Atmospheric Administration

SCC: Strongly Connected Components

SI: Source index

SLIM: Second-generation Louvain-la-Neuve Ice-Ocean Model

SR: Self-recruitment

WCL: Weighted connectivity length

WFS: West Florida Shelf

1. Introduction

1.1. General context

Ever since the Industrial Revolution, the atmospheric CO_2 concentration has been constantly increasing, mainly due to fossil fuel consumption. The best-known consequence of this rising CO_2 is global warming, but it is not the only one. Two changes that worry marine scientists are the rising ocean temperature and the acidification of the ocean. At the current rate, ocean's temperature could increase by 1-3°C by 2100, while the pH could decrease by 0.14-0.43 unit. (Hoegh-Guldberg et al. 2014).

Additionally, there has been an increase in the nutrient load to coastal zones in the recent decades. This increase in nutrients can lead to eutrophication. The rise in nutrient concentration causes an increase in the plant biomass production. The resulting accumulation and decomposition of plant debris lead to a decrease of the quantity of dissolved oxygen in the water and an increase in the production of CO_2, the latter leading to further decrease of ocean pH (Harper 1992; Wallace et al. 2014).

These changes are observed all around the world, though their magnitude differ regionally (Pörtner et al. 2014). In the Gulf of Mexico (GOM), ocean acidification has been observed in the Florida Bay (Zhang and Fischer 2014) and a warming of approximately 0.8°C of the sea surface temperature has been observed in the Florida Keys over the last century (Kuffner et al. 2015).

This obviously has an impact on many marine species. One example is the change of distribution of various species of fish and invertebrates observed by Fujiwara et al. (2019) in the GOM. Crustaceans are particularly sensitive to pH changes that can alter their ability to regulate their internal acid/base balance, which impacts the hormones and enzymes involved in molting. This can lead to deformities that can result in a reduced ability to regulate their depth and avoid predators. In addition, pH sensitivity is not necessarily the same during the different stages of crustaceans' development. For some species, the early stages are more sensitive to pH changes than the adult stages (Ceballos-Osuna et al. 2013; Kurihara 2008). A rise in temperature also impacts crustaceans' development. A high temperature can lead to a metabolism acceleration and destabilize the proteins. For some species, this leads to shorter larval stages, a higher mortality rate and smaller individuals (Kuhn 2017; Young and Hazlett 1978). Additionally, a synergic effect between acidification and warmer water has been observed for several crustacean species, that results in hypercapnia and reduction in oxygen circulation (Dissanayake and Ishimatsu 2011; Metzger et al. 2007).

Florida stone crab (*Menippe mercenaria*) is one of these crustaceans for which the impacts of both acidification and increase temperature has been demonstrated. Elevated CO_2, which leads to lower water pH, and elevated temperature have been shown to reduce larval

survivorship, particularly when those two factors are combined (Brown et al. 1992; Gravinese et al. 2018). Lower pH also results in reduced rate of embryonic development (therefore increasing the time to hatching), reduced hatching success (Gravinese 2017) and a lower position in the water column of some larval stages, which can have an impact on the larval distribution (Gravinese et al. 2019).

From an environmental point of view, understanding the behavior of the creatures living around us and how we interact with them is obviously important. The economical role of *M. mercenaria* makes the comprehension of the impacts of climate change on its distribution even more essential. Stone crab fishery occurs throughout the south-eastern United States and is especially important in Florida, where it represent an annual value of ~$ 25-30 million (Gandy et al. 2016; Gravinese 2018). The landings (i.e., the part of the catch that is put ashore) peaked in the 2000-01 fishing season with a total of 3.5 million pounds of claws statewide. Since then, the statewide landings have been decreasing, in spite of the increasing number of traps. Statewide landings for the season 2009-10 amounted to 2.4 million pounds of claws (Florida Fish And Wildlife Conservation Commission 2011). Regulations have recently been put in place, notably on the size of the crabs and the type of traps, to try to increase the population and implement a more sustainable fishery (Florida Fish And Wildlife Conservation Commission 2020). Understanding the dispersion of the stone crab larvae, the recruitment pattern and the connectivity between the different stone crab's habitats could help to further increase the sustainability of the management of the stone crab fishing industry. Despite the importance of *M. mercenaria* for Florida, very few studies describe its movement during larval stage, and none were found about the description of its dispersal.

The movements of the larvae can however not be understood solely by using field observations. The first reason for this is the larvae's morphology. Larvae are small and take on colors that allow them to blend into the background (Krimsky et al. 2009; Porter 1960). They also have a long larval stage duration (about one month) (Brown et al. 1992; Lindberg and Marshall 1984; Porter 1960). Finally, stone crabs can be found in a large area, from North Carolina to Texas, with some subpopulations in the Caribbean (Krimsky et al. 2009; Krimsky and Epifanio 2008; Lindberg and Marshall 1984). For all these reasons, it is impossible to observe and fully describe the movement of the larvae from direct observations.

Two possible alternative solutions to study larval dispersal are the use of biophysical dispersal model and genetic studies (Pineda, Hare, and Sponaugle 2007; Seyoum et al. 2021). If genetic studies allow to deduce the links between populations, they are not optimal to understand the processes behind the exchanges between those populations. It is also difficult to say if the links between populations comes from recent or historical exchanges (Cowen and Sponaugle 2009). Biophysical dispersal model can provide a more accurate picture of larval dispersal and exchanges between separated habitats at a given time. A downside is that it requires to have an ocean model with a resolution fine enough to represent the small-scale

processes happening around the topographically complex coastline and habitats. Such fine-scale simulation can be very computationally expensive. A solution is to use unstructured-mesh ocean models, which allow users to increase locally the model resolution where it is required.

Larval dispersal depends on different factors: the spawning time and place, the settlement requirements, the duration of the pelagic larval state, the survival rate of the larvae and its behavior (does it swim actively or not?) and of course the hydrodynamic (Pineda et al. 2007). To take these factors into account in a biophysical dispersal model, an hydrodynamic model must be coupled with a particle transport model. This approach has been used to model other brachyuran crabs dispersion, such as the European green crab (*Carcinus maenas*) and the blue crab (*Callinectes sapidus*) (Banas, McDonald, and Armstrong 2009; Criales et al. 2019; Peliz et al. 2007).

In this work, we will use a biophysical model to evaluate the impacts of climate change on the dispersion of the stone crab larvae on the West Florida Shelf. We will use the 3D version of the Second-generation Louvain-la-Neuve Ice-Ocean Model (SLIM, https://www.slim-ocean.be/) to simulate the hydrodynamics. To simulate larval dispersal, we will be using SLIM's Lagrangian particle tracker. Both will be described in the Method section. The 2D-version of SLIM coupled with the Lagrangian tracker has been repeatedly used to model the dispersal of different drifting materials, such as coral larvae (Dobbelaere et al. 2020; Frys et al. 2020), plastics (Critchell and Lambrechts 2016; Li et al. 2018) or seagrass propagules (Grech et al. 2016, 2018). The use of the 3D-version of SLIM to model particles movements is however new. Likewise, this is the first study on crabs conducted using SLIM.

1.2. Region of interest

The GOM is a marginal sea of the Atlantic Ocean located south-east of the United States. It is bordered by five states of the United States on the eastern and northern coasts (Florida, Alabama, Mississippi, Louisiana and Texas), five Mexican states on the western and south-western coast (Tamaulipas, Veracruz, Tabasco, Campeche and Yucatan) and Cuba on the south-east. It is connected to the Caribbean Sea by the Yucatan Channel and to the rest of the Atlantic Ocean through the Florida Straits. The region of interest for this work is the West Florida Shelf (WFS), located at the eastern edge of the GOM, from the Apalachicola Bay down the west coast of Florida and up the east coast to Miami (Figure 1).

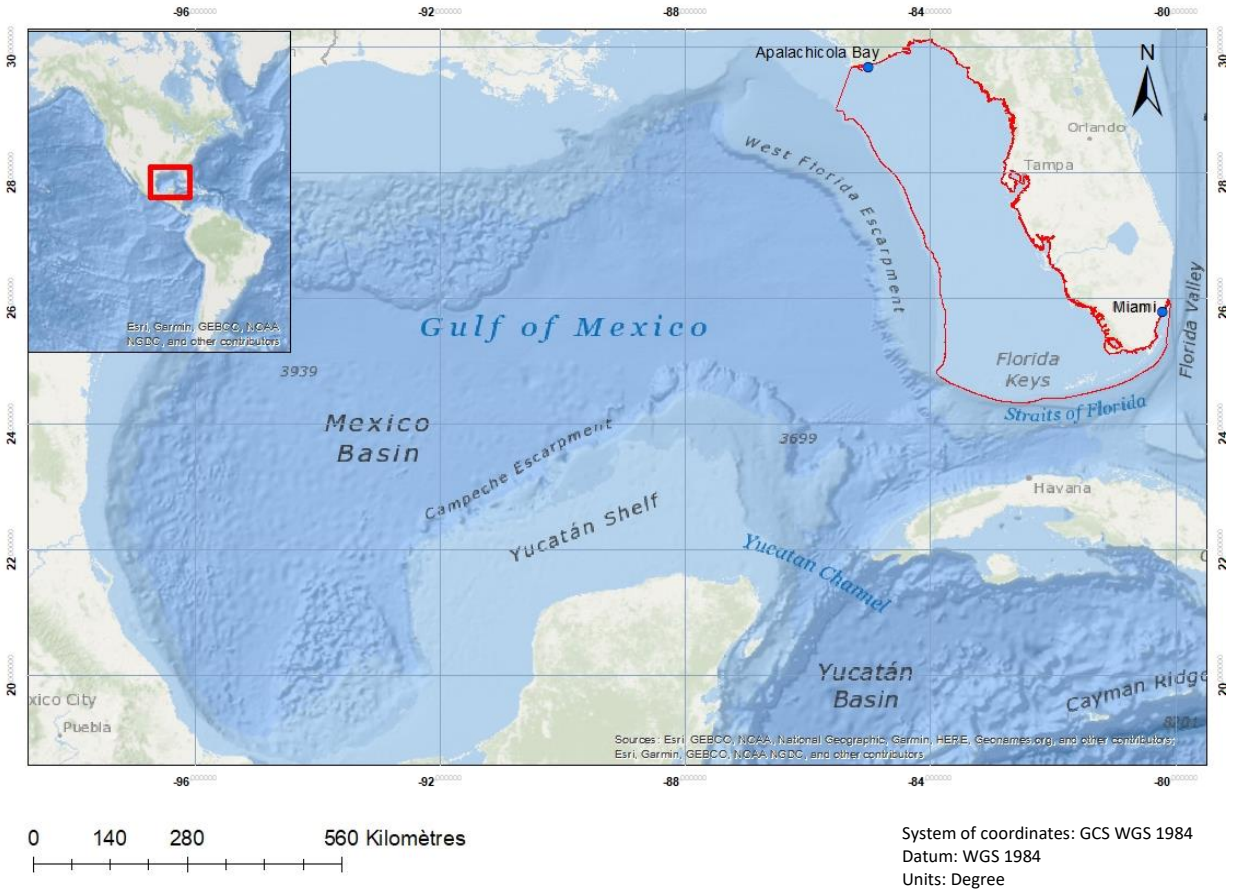

Figure 1: Map of the Gulf of Mexico. The study area is delimited in red.

The wind pattern in the GOM presents a clear seasonality. In winter, cold and dry air comes from the north to the GOM, where it meets warm and moist maritime tropical air, causing precipitations, strong winds and low average water levels. The winds coming from the south during summer are less intense. Tropical storms are however frequent during the summer, with the hurricane season ranging from August to September. On certain years, these storms can also be influenced by the El Nino phenomenon (Turner and Rabalais 2019). Winds generally blow from east to west, sometimes turning north or south when reaching the coasts depending on the season (Zavala-Hidalgo et al. 2014).

The GOM is surrounded on the Mexican and American coasts by a continental shelf, whose depth is lower than 200 meters. It consists of the WFS on the east, the Mississippi-Alabama-Florida (MAFLA) shelf and Louisiana-Texas (LATEX) shelves on the north and Campeche Bank on the south (Androulidakis, Kourafalou, and Le Hénaff 2014). This surrounding continental shelf is just 2 km wide on the south and west side but become much broader (reaching 250 km) on the north side (Turner and Rabalais 2019). The zone of interest for this study is located on the WFS where the bathymetry is not deeper than 110 meters.

The most influencing current in the eastern part of the GOM is the Loop Current that brings warm water from the Caribbean Sea (Figure 2). It enters the GOM through the Yucatan Channel and exits through the Florida Straits, where it joins the Gulf Stream (Hamilton 1990). The northward penetration of the Loop current in the GOM varies throughout the year, with the maximum penetration generally occurring during the summer months and minimum during the winter months. (Vukovich et al. 1979). Large anticyclonic eddies (or warm clockwise-spinning vortices of water) periodically detach themselves from the Loop Current and migrate westward and southward in the western part of the GOM (Martínez-López, Zavala-Hidalgo, and García 2014).

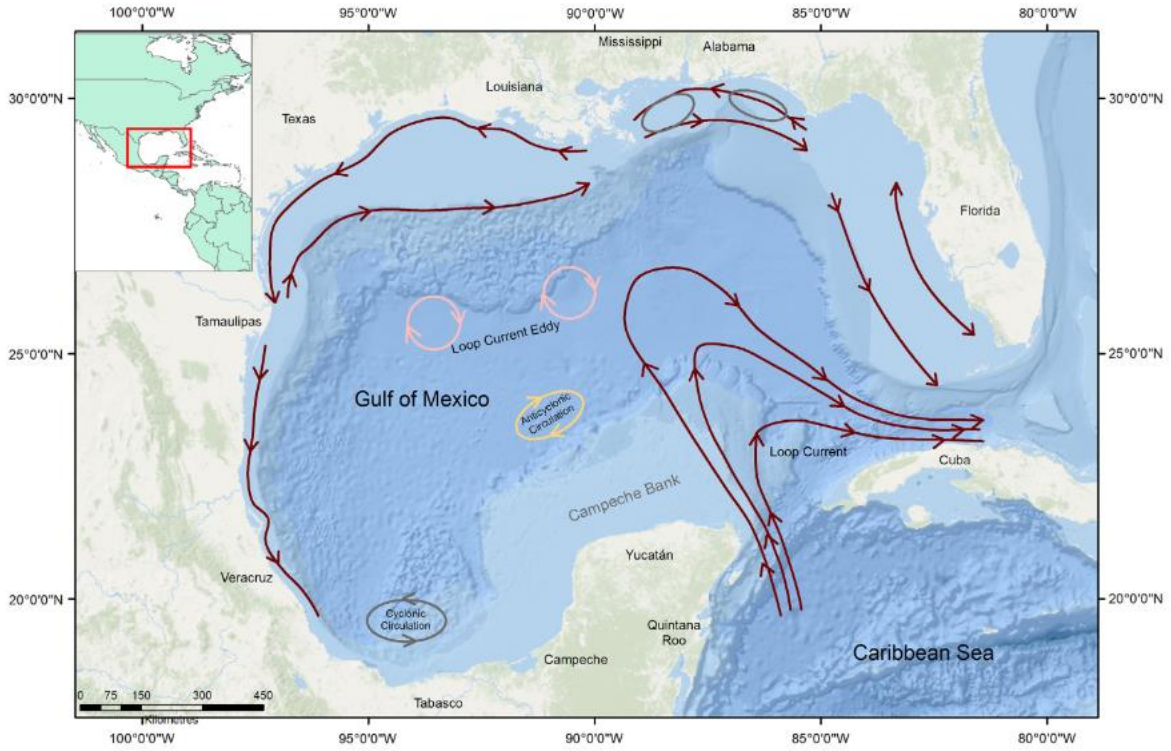

Figure 2: The Gulf of Mexico and its principal currents. Source of the figure: (Turner and Rabalais 2019)

The WFS is wide enough to have dynamical regimes different from those in the GOM, even if its dynamics remains influenced by that of the GOM. The circulation in the WFS is mainly driven by local winds but is also forced by tides, buoyancy fluxes and currents coming from the rest of the GOM, namely the Loop Current (Weisberg, Li, and Muller-Karger 2001). Just as

the GOM, the WFS is subject to seasonal changes in its circulation. The circulation in the inner shelf is mainly driven by local winds, and is predominantely downwelling-favorable during summer months and upwelling-favorable during the winter months. The amplitude and direction of the horizontal currents also present a seasonal dynamics due to the seasonal variation of the wind. On the inner shelf, the monthly mean of the currents amplitude is higher from fall to spring (2 to 12 cm/s) than during summer months (0 to 6 cm/s). The direction of the currents tends to be southeastward-directed between October and April, while the currents from June through September tend to be northwestward-directed. The seasonal variability is less pronounced from the 50 m isobath and deeper. In the outer shelf and near the southwest part of the shelf, the seasonal variations are drowned in the influences of the GOM water circulation (Liu and Weisberg 2012).

Water horizontal velocity on the WFS changes with depth. At the surface, it usually does not exceed 40 cm/s, with peaks up to 60 cm/s observed several times a year. The amplitude at depth is generally lower, although higher speeds can sometimes be observed (National Oceanic and Atmospheric Administration 2021). The direction of the currents can also vary with depth. At certain times of the year, surface and bottom currents even flow in opposite directions over significant portions of the WFS (He and Weisberg 2002, 2003).

The temperature stratification of the WFS is also worth mentionning. Like other mid-latitude continental shelves, the WFS undergoes two changes in its temperature stratification each year. In winter, the stratification is horizontal and temperature is constant throughout the water column. In summer, the stratification is vertical, with higher temperature at the surface. We can therefore observe a transition from an horizontal stratification (warmer water along the coast and homogeneous temperature in the water column) to a vertical stratification (warmer water at the surface) in the fall, and from vertical to horizontal in the spring (He and Weisberg 2002, 2003).

The population in the states bordering the GOM has been increasing steadily over the past century (U.S. Census Bureau 2020). In 2013, the number of people living in the coastal area of the GOM was estimated to 50 million (Yoskowitz et al. 2013). This steady population growth poses a threat to the coastal environments because of, among other things, the increasing flow of nutrients that is often linked to population density. (Turner and Rabalais 2019). As the population keeps on increasing, it is urgent to understand its impact on the coastal environment and try to reduce or mitigate it.

1.3. Specie of interest

Like all brachyuran crabs, *M. mercenaria* has a complex life cycle, made of four main stages (Figure 3): the larval stage, composed of a certain number of zoeal stages depending on the species, the post-larval or megalopal stage, the juvenile stage and the adult stage (Gulf Shores Marine Fisheries Commission 2001; Sulkin 1984).

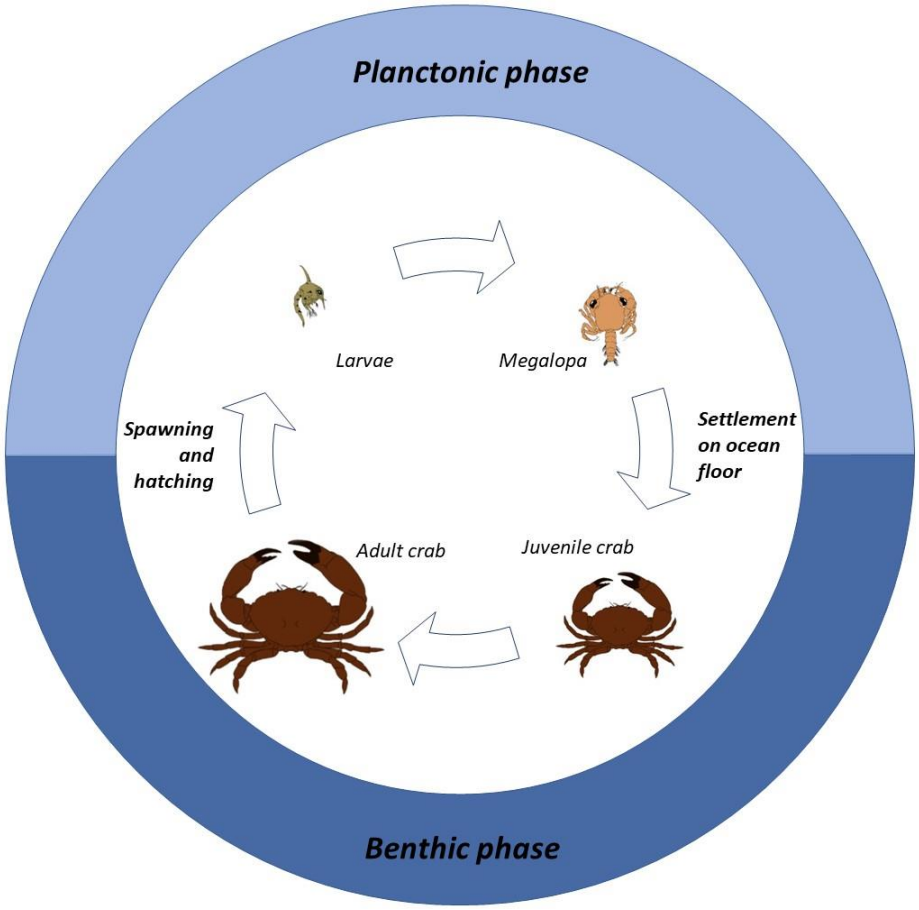

Figure 3 : Life cycle of a brachyuran crab with its 4 main stages

For stone crabs, the spawning peaks in early summer, from May to August. It can however occur all year long at a lower frequency in the south of Florida, if the temperature is above 20-22°C. The eggs remain attached to the female until hatching, after which the larvae are going to exhibit a planktonic behavior (Lindberg and Marshall 1984). The hatching occurs after 9 to 14 days and two hatching events are generally separated by 17 to 21 days (Binford 1913; Porter 1960). Larval spawning usually begins during daytime and can last for several hours, the median time being 20 hours (Krimsky et al. 2009).

After hatching, the stone crab goes through five zoeal stages, the whole process lasting 27 to 30 days. Each stage normally lasts between 3 to 6 days (Porter 1960), but these durations can drastically change with temperature (Brown et al. 1992). Larvae require warm water and

high salinity, with the highest survival rate observed in lab studies at 30°C and around 30-35 ppt respectively (Brown et al. 1992; Lindberg and Marshall 1984; Porter 1960).

One of the main factors that determines larval dispersion is larval behavior (Sulkin 1984). Crab larvae are indeed not passive drifters. They can swim vertically to position themselves in the water column. This impacts the distribution of the larvae since water movements are different with depth. Additionally, the different zoeal stages react differently to external stimuli such as hydrostatic pressure, light and gravity, therefore positioning themselves at different depths. Gravinese (2018) found that stages 1 and 3 tend to exhibit negative geotaxis (they swim upward), positioning themselves in shallower water. However, they also seem to show negative phototactic response, which means that stages 1 and 3 are migrating deeper in the water column during the day to escape light and come back to shallower water when the light intensity is low enough. This would result in greater transport of these zoeal stages during night than day. On the other hand, stages 5 larvae exhibit positive geotaxis, positioning themselves deeper in the water column. This probably allows late-stages larvae to move more easily to find appropriate settlement habitats. Like stages 1 and 3, they show a negative phototactic response to light, but it seems they are less sensitive than early larval stages. All larval stages exhibit an upward movement when exposed to an increase of hydrostatic pression, and swim downward when the pression decreases.

During the megalopal stage of their development, stone crabs transition from a planktonic behavior to living on the sea floor. After settlement, they can be found in a wide variety of substrate, ranging from rock, shell or coral rubble to oyster reefs, seaweed mats and seagrass meadows. (Krimsky and Epifanio 2008). The duration of this stage can range between one to two weeks, depending on the salinity and temperature conditions (Brown et al. 1992; Ong and Costlow 1970).

Adult stone crabs are preferably found on rocky, muddy or gravely substrates from shallow subtidal area to depth of 60m (Beck 1995; Bert, Warner, and Kessler 1978; Gravinese, personal observations; Krimsky and Epifanio 2008).

The fishery season ranges between the 15th of October and the 15th of May (Florida Fish And Wildlife Conservation Commission 2011). The fishing mostly occurs between 6 and 15 meters of water depth due to the cost associated with going far from the coast, although some fishermen work in water up until 30 m depth (Gravinese, personal observations).

Since stone crabs can live up to a depth of 60m, some of its habitats are outside of the fishing zone. In the context of a decreasing number of catches, the habitats in the non-fishing zone could potentially be a source of larvae for the habitats in the fishing zone. In which case, it would be worthwhile to include these habitats in future fishery management and crab protection plans.

1.4. Objectives

The rise in atmospheric CO_2 leads to ocean acidification and ocean warming. The commercially important Florida stone crab is one of the many species that is going to be impacted by those changes.

The main objective of this work is to answer the following questions:

- ***What will be the impacts of climate change on the dispersion of stone crab larvae on the West Florida Shelf?***
- ***Can the habitats in the non-fishing zone serve as a source of larvae for the habitats in the fishing zone?***

To answer those questions, we have identified several intermediate objectives that will allow us to build an integrated modelling sequence.

As the currents play a major role in the dispersal of the larvae, our first objective was to represent the 3D hydrodynamics of the WFS from May to September 2019. To this end, we used the 3D version of the ocean model SLIM.

We then aimed to model the dispersion of the stone crab larvae, using SLIM's Lagrangian particles tracker. The goal was to understand this dispersal thanks to the results of a connectivity study.

We finally evaluated the impact of climate change using three different scenarios.

The different steps to achieve these goals are detailed in the Methods section. We will then present our results and discuss their implications.

2. Methods

This work is divided in four parts. In the first one we used SLIM3D to model the hydrodynamics of the zone of interest. The second part consists of the model of the larval dispersal by mean of SLIM's particle tracker. A connectivity study is then conducted to evaluate the dispersion of stone crab's larvae. The last part assesses the impacts of climate change on larval dispersal.

2.2. Hydrodynamics modeling

2.2.1. Model equations

The hydrodynamic is modelled using SLIM3D, an ocean model that solves 3D hydrostatic equations under the Boussinesq approximation (Duquesne et al. 2021; Vallaeys et al. 2018). These equations can be derived from the Navier Stokes equations under the assumption that the density variations are small enough to be neglected except in the buoyancy term, and the pressure is only dependent on the height of water column and its density. The model equations read:

$$\frac{\partial \boldsymbol{u}}{\partial t} + \boldsymbol{\nabla}_h \cdot (\boldsymbol{u}\boldsymbol{u}) + \frac{\partial w\boldsymbol{u}}{\partial z} = \boldsymbol{\nabla}_h \cdot \left(\nu_h(\boldsymbol{\nabla}_h \boldsymbol{u} + (\boldsymbol{\nabla}_h \boldsymbol{u})^T)\right) + \frac{\partial}{\partial z}\left(\nu \frac{\partial \boldsymbol{u}}{\partial z}\right) - f\boldsymbol{e}_z \wedge \boldsymbol{u} - \frac{1}{\rho_0}\boldsymbol{\nabla}_h p, \quad (1)$$

$$\boldsymbol{\nabla}_h \cdot \boldsymbol{u} + \frac{\partial w}{\partial z} = 0, \quad (2)$$

$$\frac{1}{\rho_0}\boldsymbol{\nabla}_h p = \frac{1}{\rho_0}\boldsymbol{\nabla}_h p_a + g\boldsymbol{\nabla}_h \eta + \frac{g}{\rho_0}\boldsymbol{\nabla}_h \int_z^\eta (\rho - \rho_0)\, dz, \quad (3)$$

$$\frac{\partial T}{\partial t} + \boldsymbol{\nabla}_h \cdot (\boldsymbol{u}T) + \frac{\partial (wT)}{\partial z} = \boldsymbol{\nabla}_h \cdot (\kappa_h \boldsymbol{\nabla}_h T) + \frac{\partial}{\partial z}\left(\kappa \frac{\partial T}{\partial z}\right) + f_{relaxT}, \quad (4)$$

$$\frac{\partial S}{\partial t} + \boldsymbol{\nabla}_h \cdot (\boldsymbol{u}S) + \frac{\partial (wS)}{\partial z} = \boldsymbol{\nabla}_h \cdot (\kappa_h \boldsymbol{\nabla}_h S) + \frac{\partial}{\partial z}\left(\kappa \frac{\partial S}{\partial z}\right) + f_{relaxS}, \quad (5)$$

where **u** is the horizontal velocity, composed of the zonal and meridional velocity components, w is the vertical velocity, $\boldsymbol{\nabla}_h$ is the horizontal gradient operator, ν_h is the horizontal viscosity, T is the temperature, ν is the vertical eddy viscosity, f is the Coriolis factor, $\boldsymbol{e}_z$ is the vertical unit vector, ρ_0 is the reference density, p is the pressure, p_a is the atmospheric pressure, η is the elevation, ρ is the density, κ_h is the horizontal eddy diffusivity, κ is the vertical eddy diffusivity and f_{relaxT} and f_{relaxS} are respectively the temperature and salinity relaxation terms.

These equations represent the fundamental processes driving the ocean circulation. Eq. (1) is the momentum equation. It is based on the law of conservation of momentum that states that in a closed system, the total momentum is conserved. This implies that a change

in momentum in a water parcel is due to the forces acting on it. Eq. (2) is the continuity equation. It is based on the law of mass conservation, which states that the mass variation in a water parcel is equal to the difference between in- and outgoing mass fluxes through the parcel boundaries. Eq. (3) is the pressure equation. It expresses the horizontal pression gradient under the hydrostatic assumption as the sum of the atmospheric pressure, sea surface elevation and baroclinic pressure gradient. Eq. (4) and (5) are the temperature and salinity equations, respectively. They are expressed as advection diffusion equations with a surface relaxation term. This relaxation term is similar for both equations and reads

$$f_{relax\,Y} = -\frac{max(z_r + z, 0)}{z_r t_{relax}} * (Y - Y_{ext})$$

where z_r = 12 m is the surface layer thickness, t_{relax} = 5 days is the relaxation time, Y is either T or S and Y_{ext} is the value of variable Y at the ocean surface as computed by the HYbrid Coordinate Ocean Model (HYCOM). HYCOM is an ocean model where the GOM is represented with a resolution of 1/25° or ~3.5km horizontally. The aim of this relaxation term is to force the temperature and salinity computed by SLIM to remain close to the one of HYCOM near the surface. This relaxation term is required as SLIM3D does not include surface heat and salinity fluxes that depend on solar radiation and precipitation. The parameter t_{relax} is set to five days to correspond to the time scale at which temperature and salinity change. The relaxation term is at its maximum at the surface and decreases until it equals zero when depth equals to z_r.

Other parameters must be defined to use SLIM3D's equations. The horizontal viscosity v_h is parametrized by means of the Smagorinsky turbulent model, that expresses the viscosity by taking small-scale turbulent effects into account (Smagorinsky 1963). The horizontal diffusivity κ_h is defined by the Okubo parametrization, which defines the diffusivity as a function of the mesh size (Okubo 1971). The vertical counterpart of those parameters, the vertical eddy viscosity v and the vertical diffusivity κ, are computed with GOTM (General Ocean Turbulence Model), which provides a suite of vertical turbulence closure models. The Coriolis factor f is defined as a function of the latitude:

$$f = 2 \cdot \Omega \cdot sin(\varphi)$$

where $\Omega = 7.292 \cdot 10^{-5}$ radians/s is the earth rotation's speed and φ is the latitude. The atmospheric pressure, used in eq. (3), is the pressure exerted by the atmosphere, adjusted to the height of the mean sea level. In this work, it is provided by ERA5 on the Climate data store (CDS). ERA5 is the latest climate reanalysis produced by the European Centre for Medium-Range Weather Forecasts (ECMWF). It provides data on many atmospheric, land and oceanic climate variables on a 30 km grid with a 1 hour time resolution (ECMWF 2021).

2.2.2. Model forcing

Since the model equations only apply to elements within the domain, the external forcings that drives the ocean circulation in the domain are represented through boundary conditions.

The current velocity and sea surface elevation are influenced on the open boundaries by the tides and the large-scale circulation. The tides are provided by the OSU TOPEX/Poseidon Global Inverse Solution dataset TPXO9 (Egbert and Erofeeva 2002). It combines different tidal models to offer a resolution of 1/30°. The large-scale circulation in the GOM and Florida straits is computed with HYCOM-GOM. The velocities and elevation from HYCOM are then added to the tidal velocity and elevation from TPXO9 and those are imposed as open boundary conditions. The other open boundary conditions, namely the temperature and the salinity, also come from the HYCOM model.

The bottom and surface boundaries are made impermeable through the following equations:

$$w + \boldsymbol{u} \cdot \boldsymbol{\nabla}_h h = 0 \tag{6}$$

$$w - \frac{\partial \eta}{\partial t} - \boldsymbol{u} \cdot \boldsymbol{\nabla_h} \eta = 0 \tag{7}$$

There is an input of momentum at the surface from the wind and a dissipation of momentum at the bottom from friction. These two fluxes are expressed as follows:

$$\nu \frac{\partial \boldsymbol{u}}{\partial z} = \frac{\tau_s}{\rho_0} \tag{8}$$

$$\nu \frac{\partial \boldsymbol{u}}{\partial z} = \frac{\tau_b}{\rho_0} \tag{9}$$

where τ_s is the surface wind stress and τ_b is the bottom friction stress. The wind stress is derived from Smith and Banke (1975), based on the 10-m wind velocity provided by ERA5. The bottom friction is computed with the law of the wall, assuming a logarithmic velocity profile characterized by a roughness height z_0.

Initial conditions must be defined before beginning the simulation. In this work, the initial salinity and temperature are defined by taking the solutions of HYCOM. Concerning the current velocity and sea surface elevation, the initial conditions are defined as being equal to zero. This means that the model needs a few days to spin-up and reach a dynamical equilibrium. For this reason, we begin the simulation of the hydrodynamics on the 15th of April, to have stabilized currents when the simulation of the larvae begins on the 1st of May.

2.2.3. Model discretization

The model equations are discretized with the discontinuous Galerkin finite element method on a 3D mesh made of triangular prisms. The 3D mesh is obtained by extruding in the vertical an unstructured 2D mesh made of triangles. This allows us to increase or decrease the resolution spatially, which can in turn be fine-tuned to capture the small-scale processes happening in and around the most important parts of the domain. In this work the size of the mesh elements depends on the distance to the coast, the distance to stone crabs' habitats, the bathymetry and the bathymetry gradient. The bathymetry is extracted from the Coastal Relief Model, which offers a representation of the US coast with a resolution of 3 arc-seconds, or roughly 90 m (NOAA National Geophysical Data Center 2001).

At the moment there are no stone crab habitat maps. However, stone crabs are known to prefer rocky, muddy or gravely substrate up to depth of 60 m (Beck 1995; Bert, Warner, and Kessler 1978; Gravinese, personal observations; Krimsky and Epifanio 2008). We therefore decide to use a seafloor substrate map of the GOM and to consider that areas above 60 m depth where the substrate is either rock, mud or gravel dominant, correspond to areas where the stones crabs live. The seafloor substrate map was made by the Institute of Arctic and Alpine research of the University of California and has a resolution of 4km^2 (INSTAAR 2011).

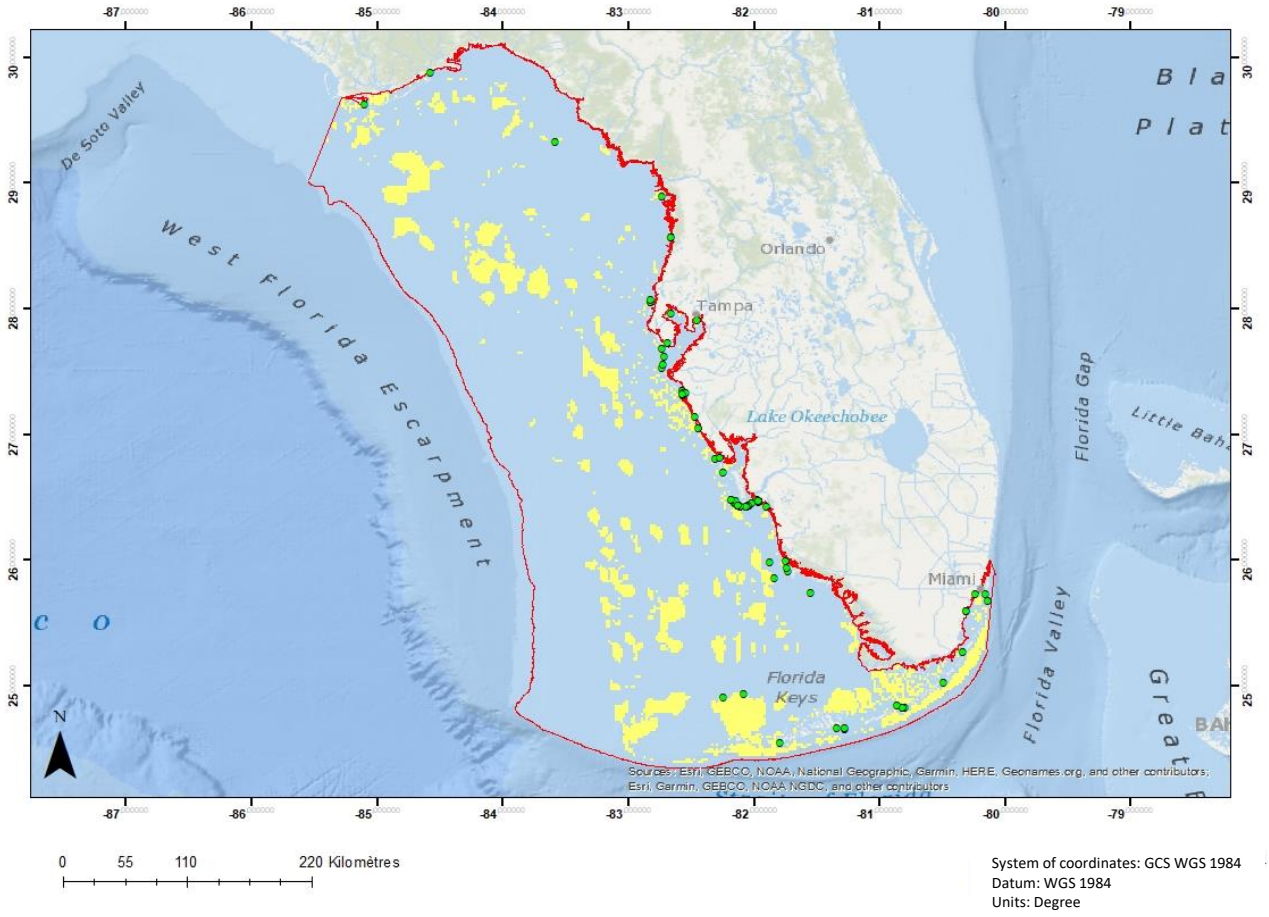

Figure 4 : Habitats preferred by stone carbs in the West Florida Shelf (yellow polygons) locations where stone crabs were observed between 2011 and 2021 (green dots).

The selection of habitats was validated by looking at punctual observations reported on the Global Biodiversity Information Facility (GBIF) between 2011 and 2021 (GBIF Backbone Taxonomy 2019) (Figure 4). As a result, we have 3858 habitats patches of 4 km^2.

In this work, the horizontal mesh resolution is higher along coastlines and over crab habitats, as well as where the bathymetry is shallow or steep. The resulting mesh is composed of about 34 000 elements, whose size ranges from about 400 m to 10 000 m (Figure 5).

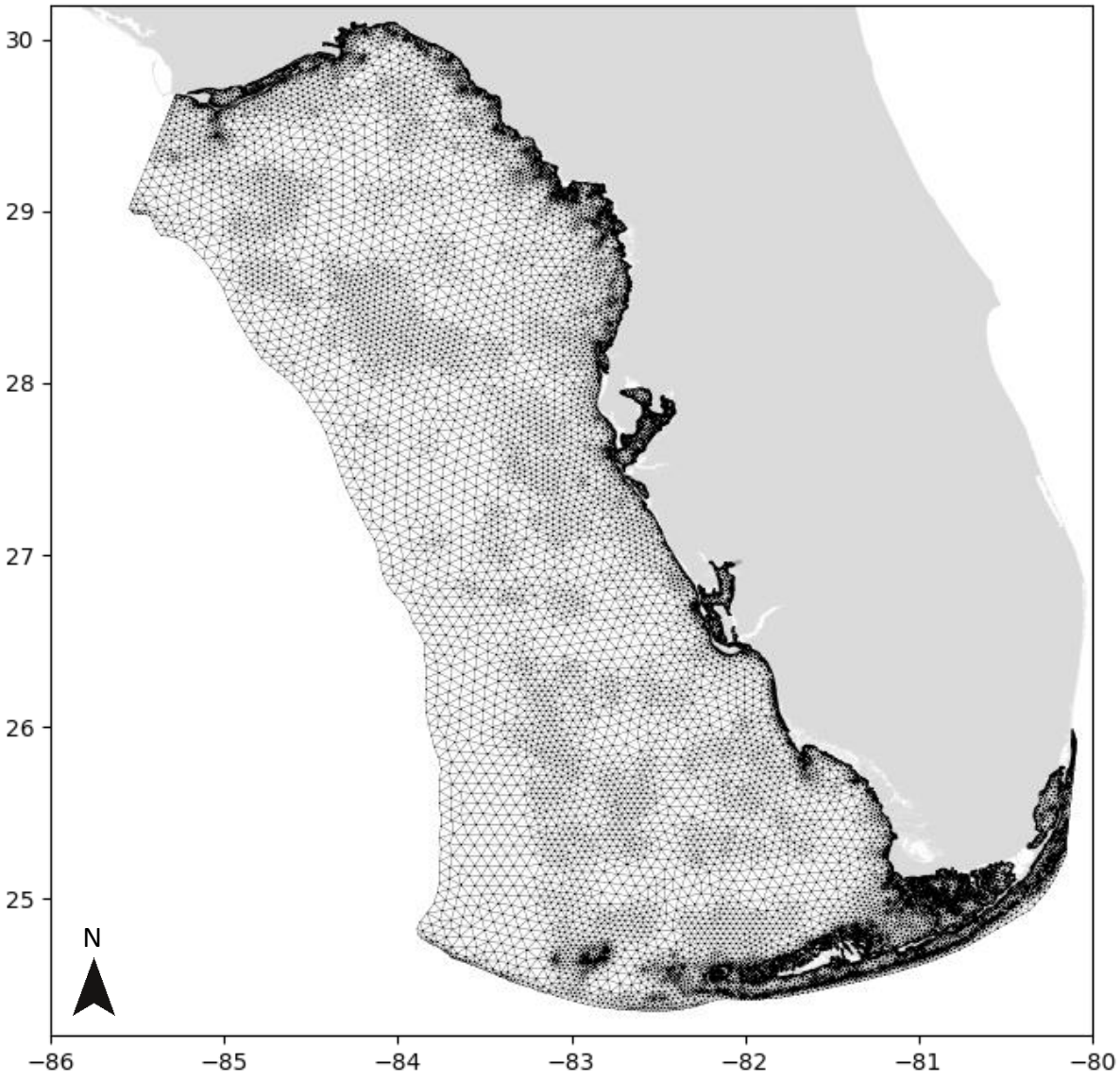

Figure 5 : Horizontal mesh of the computational domain. The black lines represent the limits between the elements, the gray area is the mainland. The mesh resolution ranges from 400 m to 10 km.

The vertical layers in SLIM3D can be defined using a combination of *z* and *σ* coordinates. Both of these have advantages and disadvantages.

With *σ* coordinates, a fixed number of layers follow the ocean's floor, therefore allowing for a smooth representation of the ocean bottom. However, the discretization in *σ* coordinates can introduce internal pressure gradients errors, especially where the bathymetry gradient is steep. This is due to the fact that the layers are generally not horizontal. With *σ* coordinates, the pressure gradient force is determined by summing the gradient of pressure along a fixed σ surface and a term involving the gradient at the bottom of the sea. When the bathymetry is steep, those two terms are large and of opposite signs, roughly cancelling each other. However, a small error in one of those terms can cause a large error in the estimation of the pressure gradient force.

With *z* coordinates, the layers do not follow the bathymetry, but correspond to horizontal levels set at fixed depths, creating a staircase-like representation of the ocean bottom. The number of layers is therefore not constant throughout the domain and depends on the bathymetry at each point. The disadvantage of *z*-levels is that a high number of levels is necessary near the bottom to obtain an accurate representation of the ocean floor, which requires an important computation time. On the other hand, no error on the pressure gradient is introduced.

Due to these differences, the *σ* discretization is generally preferred in shallow environment with mild bathymetry gradients, while the *z* discretization is used in deeper areas where the bathymetry is steeper. (Delandmeter et al. 2018; Haney 1991; Vallaeys et al. 2018). In this work, we only use the *σ* coordinates as the bathymetry of the WFS does not exceed 110 meters and its gradient is rather small. Layers are more tightly packed near the surface than near the bottom to better represent the wind-driven surface mixed-layer dynamics (Figure 6). There are 20 layers in total, their size increasing with depth every five layer. As a result, we have at the deepest locations 5 layers in the top 11 meters, achieving a resolution of at least 2.2 m near the surface.

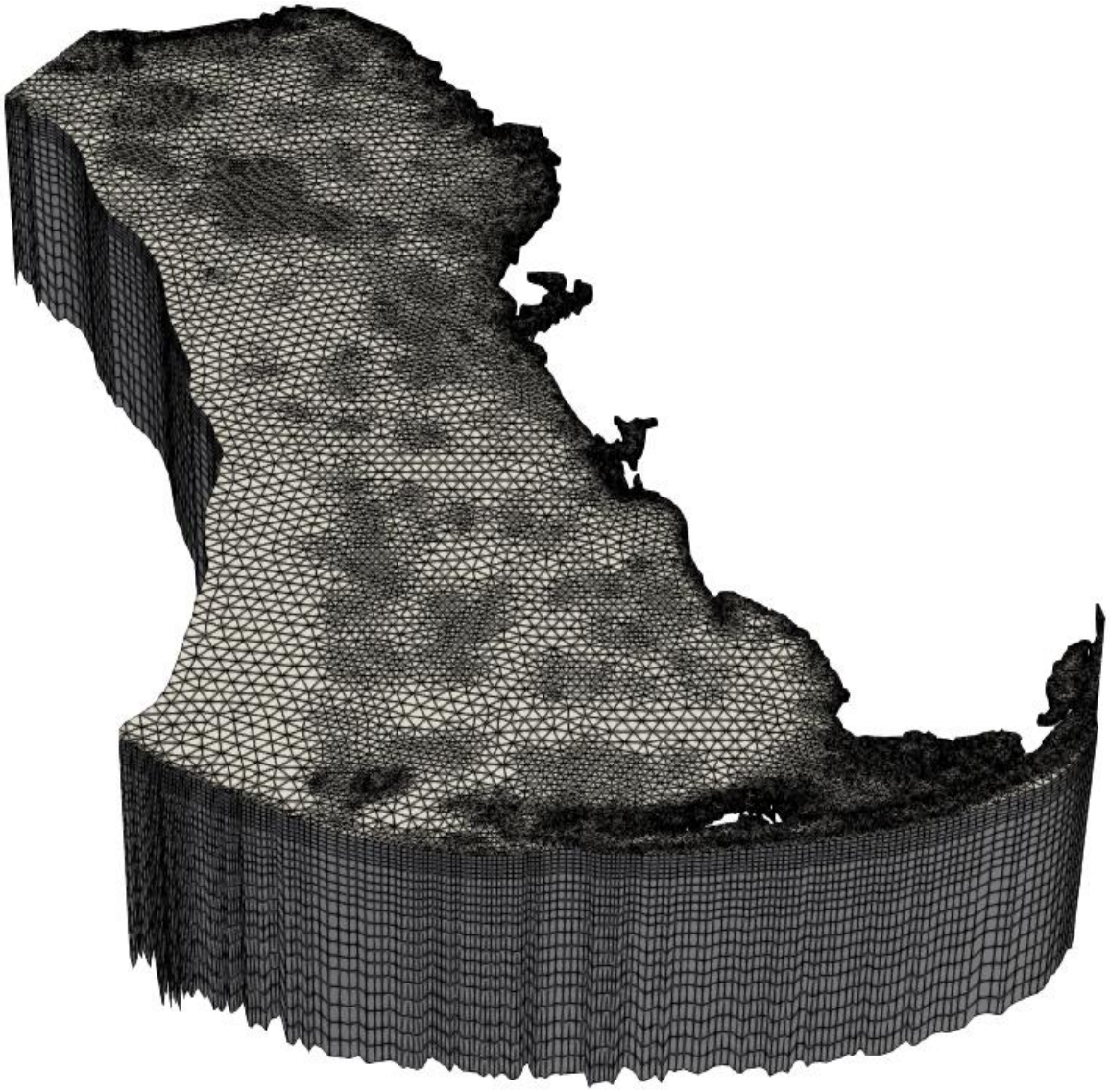

Figure 6 : 3D-mesh of the computational domain There are 20 σ levels. The dark black lines represent the limits between elements.

2.2.4. Model validation

The hydrodynamic model outputs are compared with data from three stations of the National Oceanic and Atmospheric Administration (NOAA) (Figure 7). The water velocity outputs are compared to the observations at a 4 m depth of the station 42023 (26.010° N, 83.086° W). The comparison covers the velocity amplitude over time, as well as the histograms of both velocity directions and amplitudes. Concerning the temperature and salinity, the outputs are compared with the observations made at a 1 m depth by station 42013 (27.173°N, 82.924°W), and station 42022 (27.505°N, 83.741°W), respectively. The validation is made by comparing the observations (without the missing values) and the outputs of the model over time. A vertical transect of temperature and salinity outputs of the model is also checked over time, to validate that there are no sudden changes in the stratification. The stations were chosen because they presented the fewest number of missing values during the study period for each of the three variables.

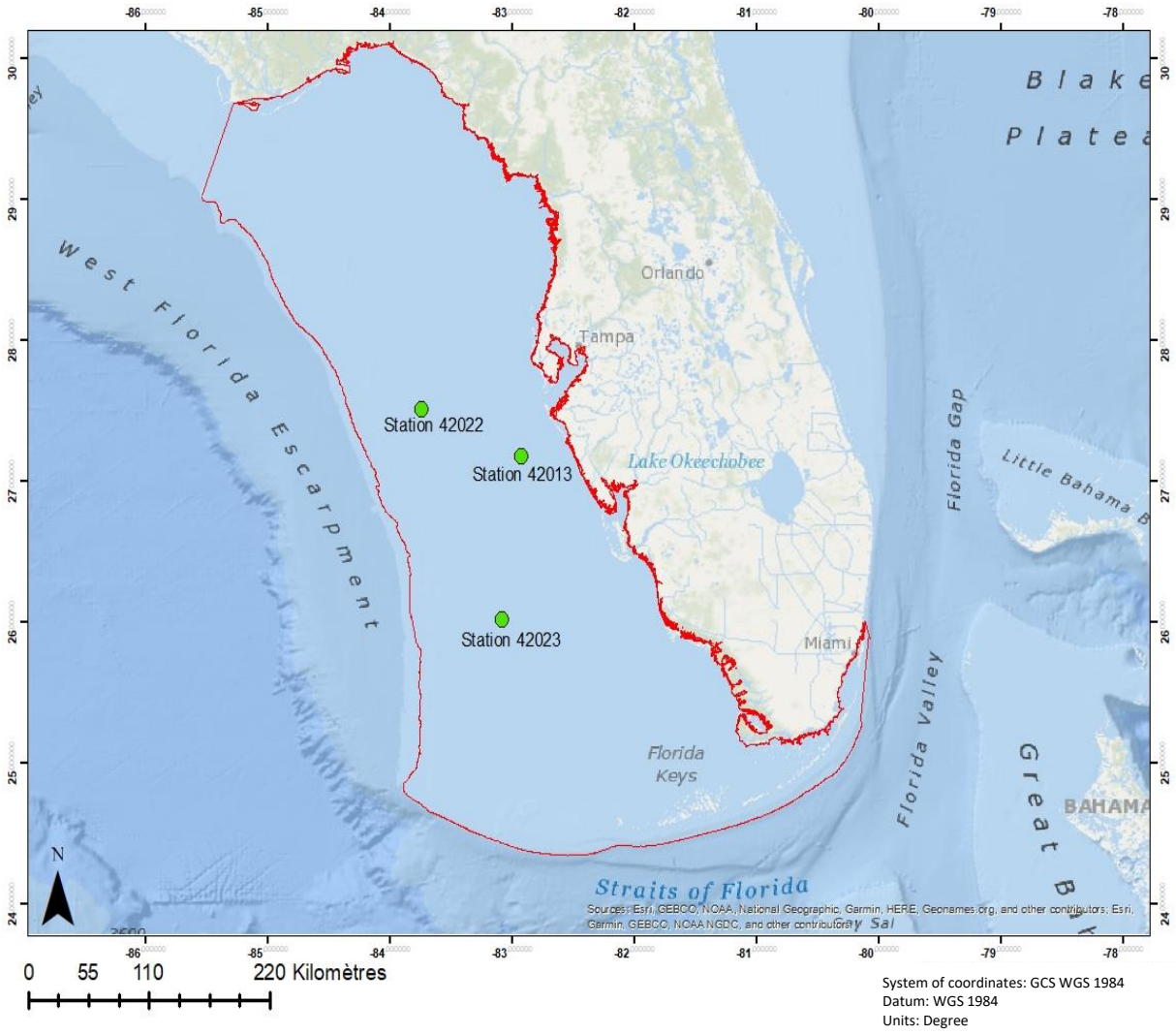

Figure 7 : NOAA stations used to validate the hydrodynamic model.

2.3. Larval dispersal

2.3.1. Lagrangian model

After modelling the hydrodynamics, the next step is to model larval dispersal. To do so, we use SLIM's Lagrangian particle tracker (LPT). The main advantage of this model is that it is object-based, meaning that each particle has its own characteristics and behavior. This allows us to implement different swimming behaviors more easily. A second advantage is that the starting and ending location of each particle released in the domain is known, which allows us to easily measure the connectivity between habitats (Thomas et al. 2014).

The movement of the particles is obtained by combining the larval swimming velocity with the currents velocity to obtain $\boldsymbol{u_L}$, the total larval velocity. This velocity vector is then injected in a 3D advection-diffusion equation expressed in Lagrangian form:

$$d\boldsymbol{X}(t) = (\boldsymbol{u_L} + \boldsymbol{\nabla \cdot K})dt + \sqrt{2\boldsymbol{K}}d\boldsymbol{W}(t) \quad (10)$$

where the advection part, in red, is defined by $\boldsymbol{u}$ and the diffusivity tensor $\boldsymbol{K}$, that reads

$$\boldsymbol{K} = \begin{bmatrix} \kappa_{L,h} & 0 & 0 \\ 0 & \kappa_{L,h} & 0 \\ 0 & 0 & \kappa_L \end{bmatrix}$$

where $\kappa_{L,h}$ is the horizontal diffusivity and κ_L is the vertical diffusivity. Like for the temperature and salinity diffusivity, $\kappa_{L,h}$ is defined by the Okubo parametrization:

$$\kappa_{L,h} = \alpha \cdot \Delta^{1.15},$$

where $\alpha = 2 \cdot 10^{-4}$ $m^{0.85}/s$ and Δ is the mesh size. The vertical diffusivity is the same as in the hydrodynamic model. The blue part of Eq. (10) defines a random diffusion, where $d\boldsymbol{W}(t)$ is a Wiener noise increment. In practice, this translates into a random walk: we take a random number between -1 and 1 and multiply it by the square root of $2\boldsymbol{K}dt$ (Gräwe and Wolff 2010). Eq. (10) is then solved numerically by the means of a 4th order Runge Kutta scheme.

2.3.2. Biological behavior

The first step in the simulation is the spawning of the larvae. The first spawning is set on the 1st of May 2019 at 14:00. Two spawning events are separated by 21 days, and the last one is set on the 4th of September 2019. Each event lasts for 20 hours, with a release of larvae every hour, with a 1 larva/km^2 density. The larvae are released 1 m above the crabs' habitats as defined in Figure 4.

Thanks to the object-based nature of SLIM's LPT, each particle can individually react to external stimuli. This means that they can have different larval stage duration, survival rates

and swimming behavior according to physical variables such as the temperature, salinity, pH or hydrostatic pressure.

We use results from Brown et al. (1992) to determine the duration of each larval stage according to temperature. We only used data for larvae that hatched from eggs developed at sea, as they seemed more representative of the modeled situation. A general multivariate regression model was performed to obtain equations that give the duration of each larval stage as a function of temperature. (Figure 8). The resulting regression has an adjusted R-squared value of 0.95 and the F-test gave a p-value of $9.2 \cdot 10^{-8}$. For the simulation of the larvae dispersion, we decided to use the temperature at the beginning of each stage to determine the duration of this stage.

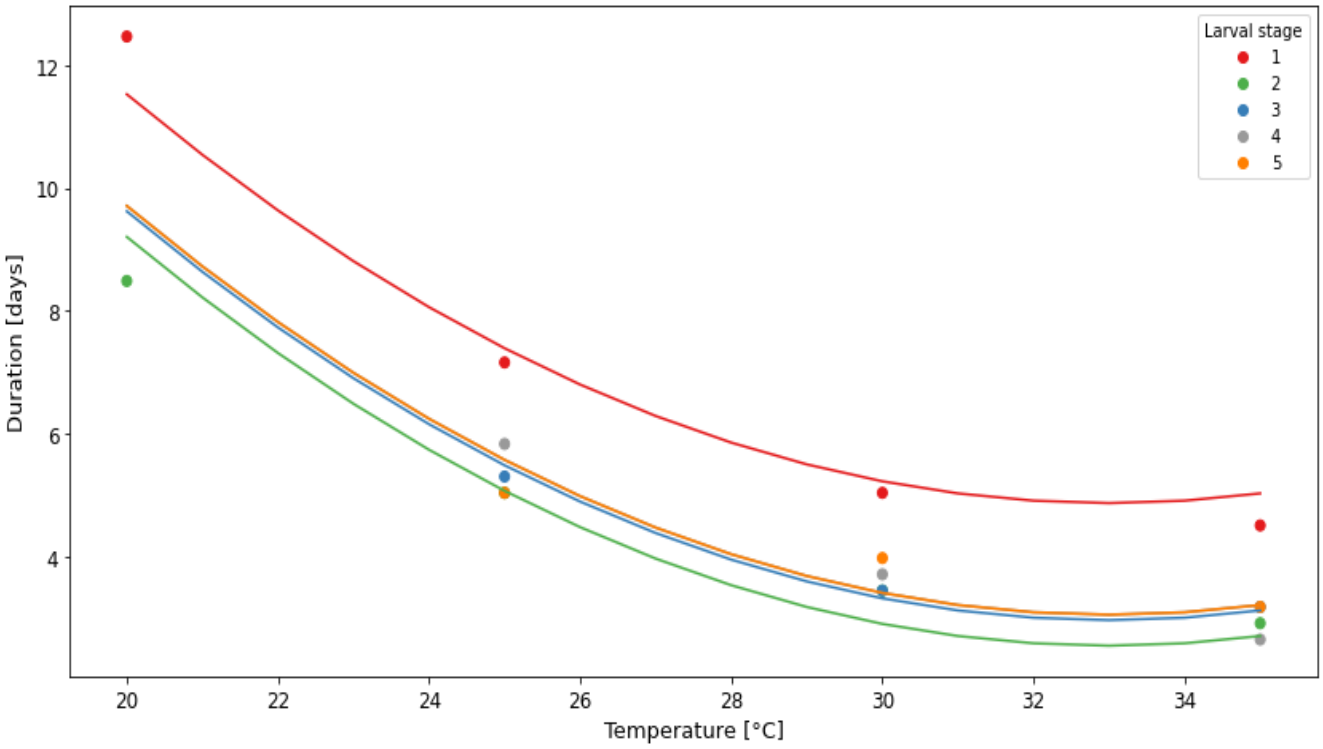

Figure 8 : Duration of each larval stage according to temperature. Circles represent observations made by Brown et al. (1992), lines represent the regressions used in this work based on the observations. Regressions for stages 4 and 5 give the same equations and cannot be distinguished on this graph.

Survival rates also change with temperature, as observed by Brown et al. (1992) and Gravinese et al.(2018). We used the former's data to derive equations describing the survival rate of each stage, according to temperature (and salinity for the first larval stage) by using a general linear model (Figure 9). The proportion of surviving larvae is calculated at the end of each stage.

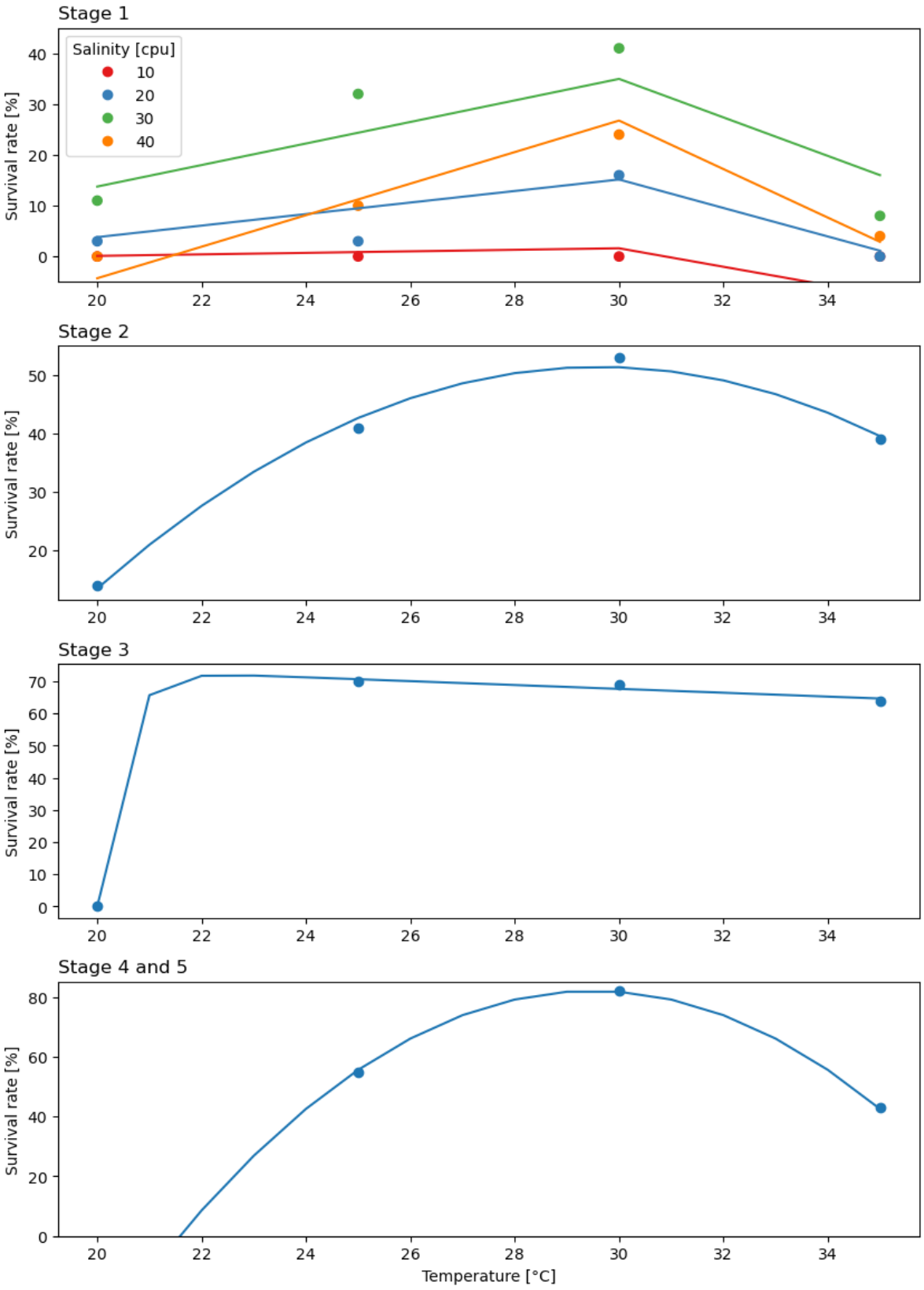

Figure 9 : Model of survival rate of each larval stage. Circles represent observations made by Brown et al. (1992), lines represent the regressions used in this work based on the observations. The first graph shows survival rate of stage -1 larvae according to salinity and temperature (R^2_A = 0.83, p-val < 0.001). The second graph shows survival rate of stage -2 larvae according to temperature (R^2_A = 0.98, p-val = 0.09). The third graph shows the survival rate of stage -3 larvae according to temperature (R^2_A = 0.997, p-val = 0.003). The last graph shows survival rate of stages -4 and -5 larvae according to temperature (R^2_A = 0.998, p-val = 0.01).

Larval vertical swimming is also affected by external stimuli. Two main methods to represent the vertical movements of the larvae can be found in the literature. The first one is to use experimental data coming from lab studies to estimate the vertical velocity (Banas et al. 2009). The second one uses the vertical distribution for each stage, obtained by vertically stratified plankton surveys, to estimate the probability for each stage to be found at a certain depth (Criales et al. 2019). A combination of these two methods can be used by restricting experimentally-derived velocities by the depth distribution of the larvae (Peliz et al. 2007).

We use the first method in this study since no depth distribution of the different larval stages was available. We model larval vertical movements according to three external stimuli, based on Gravinese experimental data: light, hydrostatic pressure and pH (Gravinese 2018; Gravinese et al. 2018). The biological component of the vertical velocity of the larvae w_B can therefore be expressed as:

$$w_B = \alpha_p \cdot (w_d + w_{Li} + w_{pH})$$

where α_p is a corrective factor due to a response to pressure, w_d is the downward swimming velocity and w_{Li} and w_{pH} are the vertical velocity in response to light and pH respectively. Since the different stages react differently to external stimuli, we define the vertical velocity of each stage separately (Table 1).

Table 1 : Components of the vertical velocity of the different life stages considered in this work.

Life stage	Vertical velocity [m/s]
Larval stage 1	$w_L = w_{B,1} + w_W = \alpha_{p,1} \cdot (w_{Li,1} + w_{pH,1}) + w_W$
Larval stage 2	$w_L = w_{B,2} + w_W = \alpha_{p,2} \cdot (w_{Li,2} + w_{pH,2}) + w_W$
Larval stage 3	$w_L = w_{B,3} + w_W = \alpha_{p,3} \cdot (w_{Li,3} + w_{pH,3}) + w_W$
Larval stage 4	$w_L = w_{B,4} + w_W = \alpha_{p,4} \cdot w_{d,4} + w_W$
Larval stage 5	$w_L = w_{B,5} + w_W = \alpha_{p,5} \cdot w_{d,5} + w_W$
Megalopal stage	$w_L = w_{B,M} + w_W = w_{d,M} + w_W$

Larvae's response to light is defined by using the time of the day. Larval stages 1 to 3 are going up during the night (between 18:00 and 06:00) and down during the day (between 06:00 and 18:00). Similar approaches have been used in other studies that takes daily migration of crabs larvae into account (Banas et al. 2009; Peliz et al. 2007). However, unlike those studies, we do not use fixed velocities during the day/night, but define a vertical velocity that changes throughout the day:

$$w_{Li} = \left(w_{d,i} - \left(w_{u,i} - w_{d,i}\right) \cdot \left(\left(\Delta t_m // (12 \cdot 3600)\right)\%2\right)\right) \cdot sin\left(\frac{2\pi}{24 \cdot 3600} \cdot (\Delta t_m)\right) \quad (11)$$

where $w_{d,i}$ is the mean downward velocity of stade i larvae according to Gravinese (2018), $w_{u,i}$ is the upward swimming velocity of stage i, $\Delta t_m = t_m - 6 \cdot 3600$ in which t_m is the time since midnight in seconds, // is the floor division operator and % is the modulo operator. This allows us to obtain a vertical velocity close to what we would have obtained, had we tried to define velocity as proportional to light intensity (Figure 10). The objective is to build a more realistic representation of biological behavior than a binary definition of velocity. Larval stages 4 and 5 vertical velocities do however not depend on light ($w_{Li} = 0$).

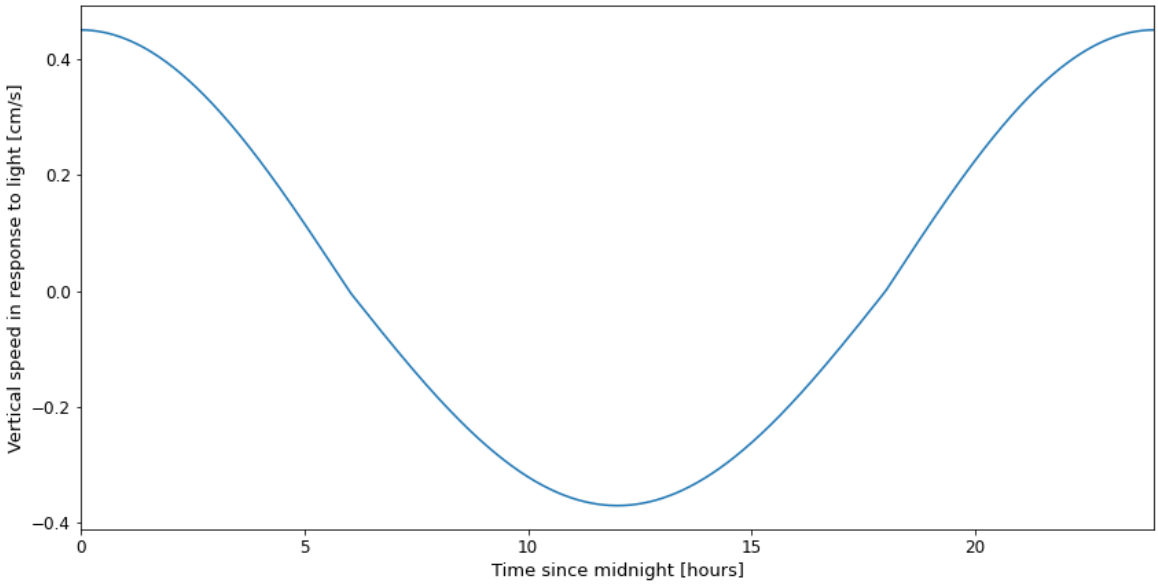

Figure 10 : Daily evolution in vertical velocity of stage 1 larvae in response to light, according to our model

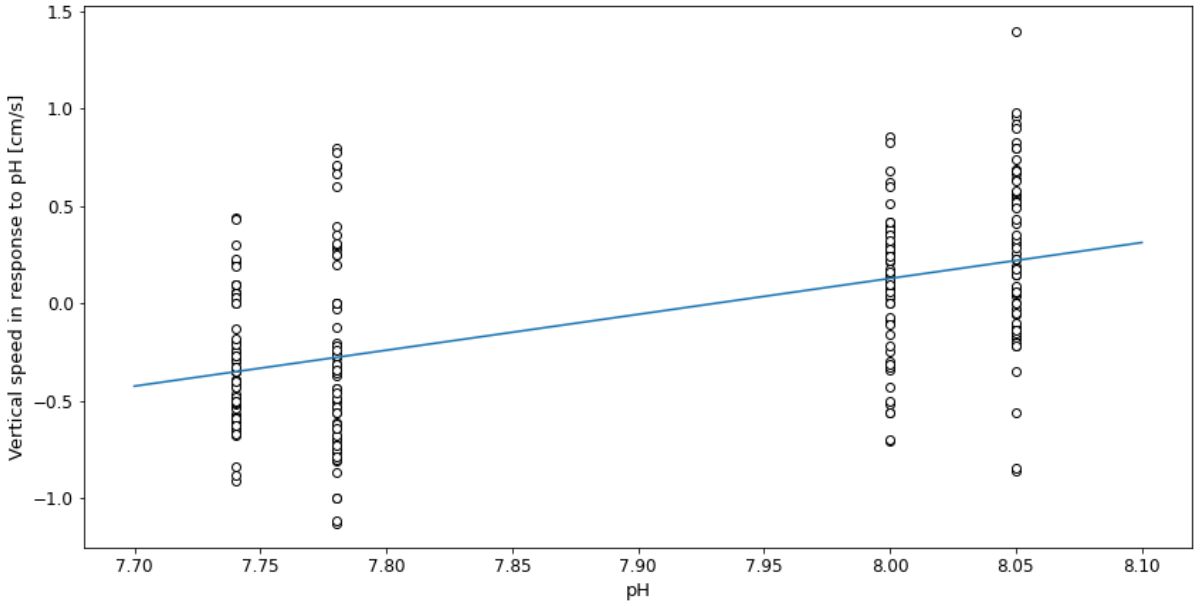

Figure 11 : Vertical speed according to pH. The circles are the observations made by Gravinese et al. (2018) for stage 3 larvae. The line is the linear regression used in this work to define vertical speed in response to pH for larval stages 1 to 3.

The vertical velocity in response to pH is defined based on observation made by Gravinese et al. (2018). They observed that stage 3 larvae swimming behavior changes with pH, while swimming behavior of stage 5 larvae does not. We impose an identical pH-dependent vertical velocity for all stages before stage 3 (Figure 11). Larval stages 4 and 5 vertical velocities do not change with the pH ($w_{pH} = 0$). The equation determining the vertical velocity according to pH for stages 1 to 3 is obtained by doing a linear regression based on Gravinese et al. (2018) data:

$$w_{pH} = (-14.64 + 1.846 \cdot pH)/100$$

The F-test of this linear regression give a p-value of $3 \cdot 10^{-22}$. We set the pH for normal conditions to 8.075 since pH varied between 8 and 8.15 in 2020 on the WFS (NOAA Ocean Acidification Program 2020).

All larval stages respond to swift changes in pressure. According to Gravinese (2018), at a rate of 0.1 mbar/sec, stages 1, 3 and 5 react respectively to a pressure increase of 80 mbar, 60 mbar and 100 mbar. At the same rate, stages 1 and 3 react to a 60 mbar and 100 mbar decrease, respectively. Based on these observations, a first model was built, taking for each larva the pressure of past positions into account. Unfortunately, this method was quite expensive in computational time. We thus opt for a simpler method, which consists in multiplying the different components of $\mathrm{w_B}$ by a corrective factor $\alpha_{p,i}$, as can be seen in Table 1. This factor is specific to each stage and is defined by functions developed to obtain velocity and depth evolutions similar to those obtained with the first model. These functions can be found hereafter (Eq. 12). Since we have no information on stages 2 and 4, it is decided to use the same $\alpha_{p,i}$ than stages 3 and 5 respectively.

$$\alpha_{p,i} = \begin{cases} \dfrac{1}{2 + exp\left(10^5 \cdot \left(\mathrm{w_L} + \mathrm{w_{pH}} - 0.0005\right)\right)} + 0.5 & , i = 1 \\ -exp\left(-\dfrac{\left(\mathrm{w_L} + \mathrm{w_{pH}} + 0.0016\right)^2}{2 \cdot 0.0005^2}\right) + 1 & , 2 \leq i \leq 3 \\ -1.18 \cdot \left|sin\left(\dfrac{\pi}{0.2776 \cdot 3600} \cdot t\right)\right| + 1 & , 4 \leq i \leq 5 \end{cases} \quad (12)$$

The correction factor for stages 1 to 3 is set as a function of the biological component of the velocity, $\mathrm{w_L} + \mathrm{w_{pH}}$. For stages 4 and 5, this component is equal to $\mathrm{w_d}$, which is a constant. However, in the first version of the model the larvae went up periodically to slow down their descent. We therefore decide to put a correction factor as a periodic function of time. As a result of the multiplication of the larvae vertical velocity by the correction factor, the changes in depth of the larvae are slowed down (Figure 12).

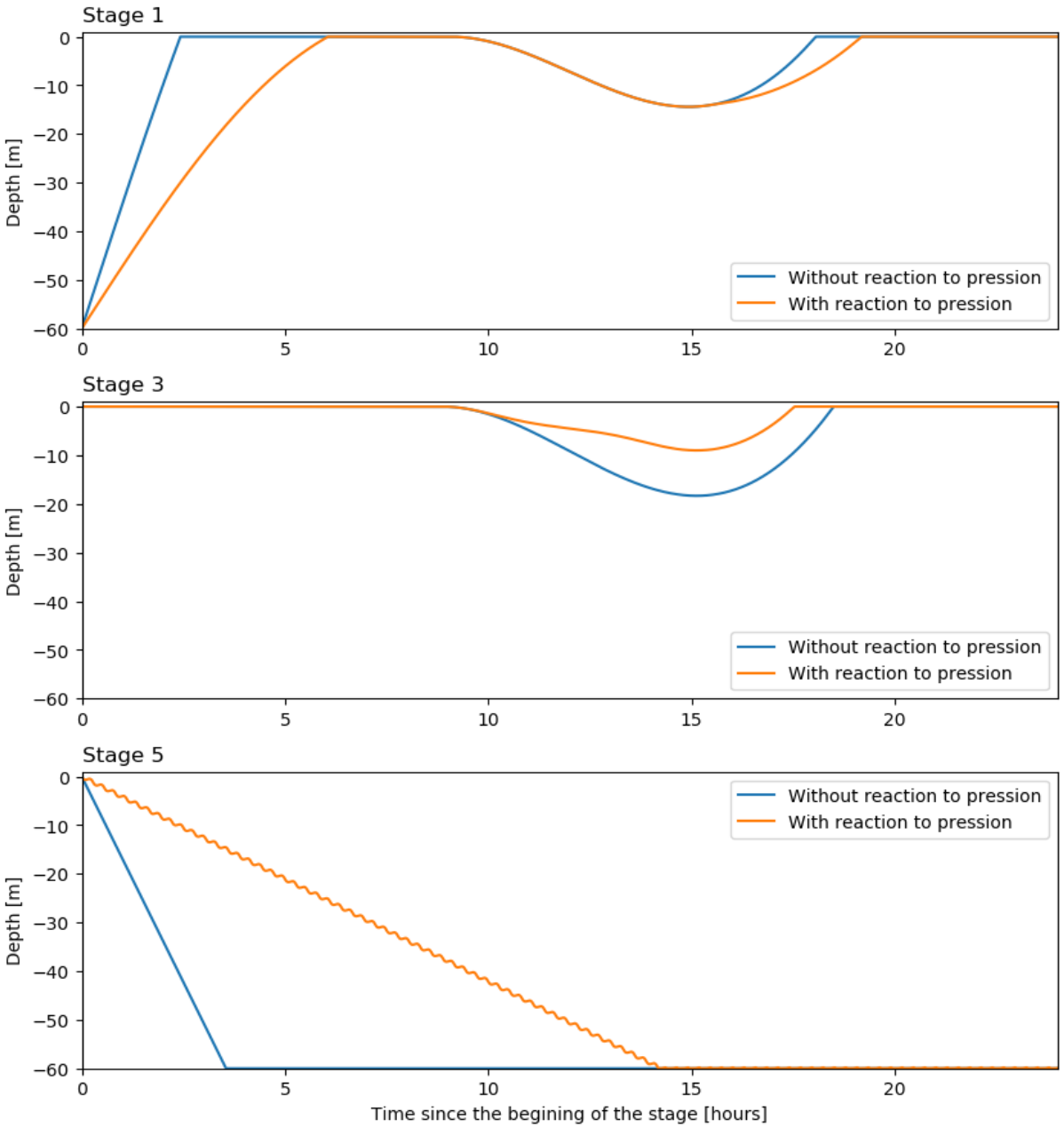

Figure 12 : Impact of the corrective factor $\alpha_{p,i}$ on the depth evolution of larval stages 1, 3 and 5 for the 24 first hours of each of these stages. The blue line represents the depth of the larva without the corrective factor, meaning that it is not impacted by changes in pression. The orange line represents the depth evolution with the corrective factor.

The megalopal stage is the one during which the crabs settle down on the ocean floor. No information was available concerning the vertical velocity of this stage. We defined its vertical velocity as being equal to the mean downward swimming velocity of stage 5 larvae, as observed by Gravinese (2018). The biological component of the vertical velocity of the megalopal stage is therefore equal to $w_B = w_{d,M} = -0.47$ cm/s. The duration of this stage is set to 13 days, as it is the longest duration observed for this stage by Brown et al. (1992). If the megalopa finds itself one meter or less above an habitat during that time, it will settle down on that habitat. If the megalopa has not settled down after those 13 days, it dies and is removed of the simulation.

2.4. Connectivity indicators

This section aims at describing how habitat connectivity is obtained from the larval dispersal simulations. This allows us to understand the way larvae are transported over the WFS.

All the analyses in this section are based on the connectivity matrix (CM) produced by SLIM's LPT. This connectivity matrix is a square matrix, in which each element C_{ij} is the connectivity between the source habitat *i* and the sink habitat *j*. What we call connectivity here is the number of particles released on habitat *i* that settles on habitat *j*. The sum of all the elements of row *i* is therefore the number of particles coming from habitat *i* that settled somewhere, whereas the sum of all the elements in column *j* is the number of larvae that settled on habitat *j*. The CM in this study has a dimension of 3858 x 3858, as we consider all the habitats in the domain.

The connectivity between each habitat *i* and *j* then needs to be normalized, to allow us to compare CM of different runs. Indeed, since there is a stochastic part in the LPT model, we need to ensure that the differences we observe are not caused by this stochasticity. There are two places in the model where this randomness intervenes, meaning that there are two ways to normalize the CM. The first one is to divide the connectivity between habitats *i* and *j* by the number of larvae seeded on habitat *i*, to remove the stochasticity occurring in the seeding process:

$$\tilde{C}_{ij} = \frac{C_{ij}}{S_i} \tag{13}$$

where $\tilde{C}_{ij}$ represents the normalized elements of the CM and S_i is the number of particles seeded by habitat *i*. The other way is to divide the connectivity by the number of larvae settling on habitat *j*, to remove the impact of the random diffusivity during the particle transport:

$$\tilde{C}_{ij} = \frac{C_{ij}}{\sum_j C_{ij}} \tag{14}$$

In this work use the first method (Eq. 13), as the objective is to measure the differences in the number of settled larvae between different scenarios.

One of the aims of this part is also to evaluate if the habitats in the non-fishing zone could be used as a source of larvae for the habitats in the fishing zone. To answer that question, we first need to distinguish the two zones. We divide the domain in two, following the 30m depth isobath, as the fishery does not occur past that point (Figure 13). We then look at each possible relation between the different habitat type (larvae going from fishing zone to fishing zone, non-fishing zone to non-fishing zone, fishing zone to non-fishing zone and non-fishing zone to fishing zone) and calculate the proportion of total settled larvae associated with each one of these relations.

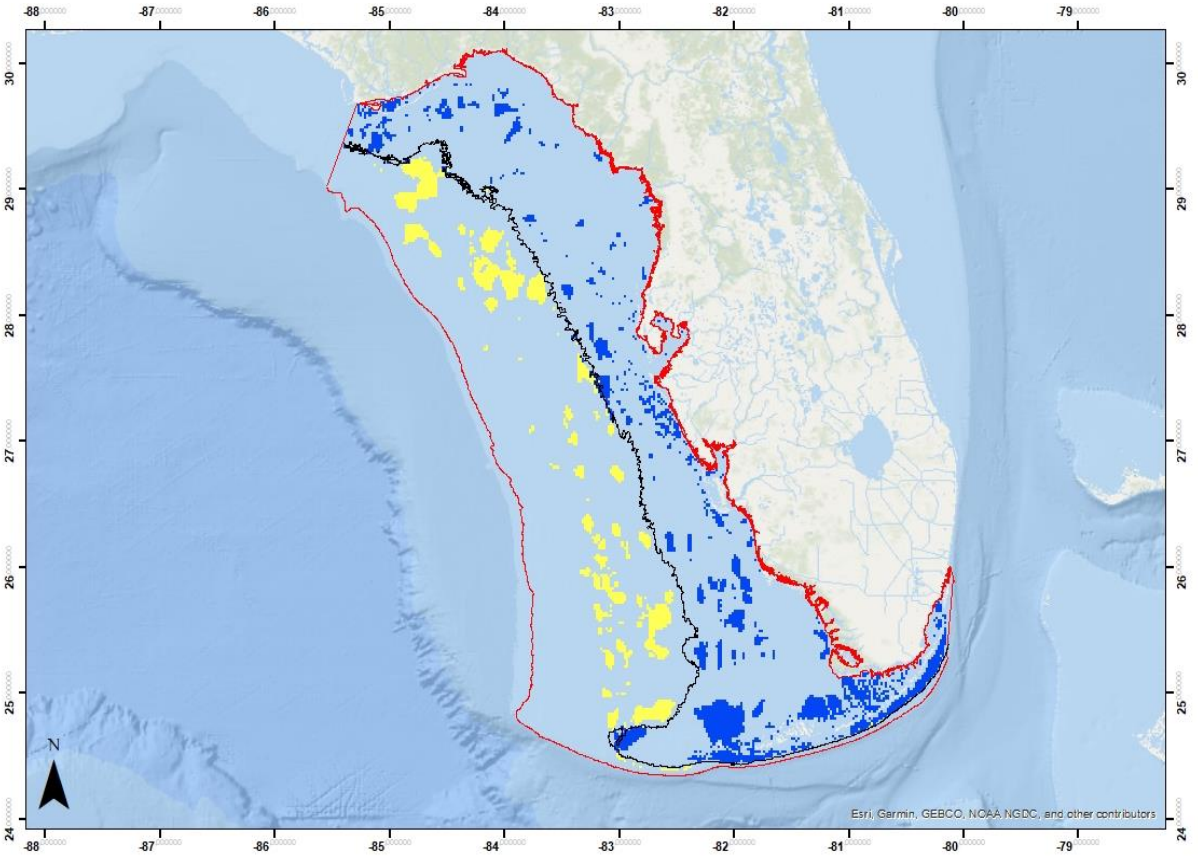

Figure 13 : Separation of the stone crabs' habitats between those in the fishing zone (dark blue) and those outside the fishing zone (yellow). The red line represents the boundaries of the domain, and the black line is the 30m depth isobath that separates the fishing and non-fishing zones.

The CM can also be used to compute different indices. We focus on two of them, the weighted connectivity length and the source index, as they are the most relevant for our study. The weighted connectivity length (WCL) of habitat *i* is the average dispersal distance of the larvae released by habitat *i* to a destination habitat. It is calculated as:

$$WCL_i = \frac{\sum_j \tilde{C}_{ij} \cdot d_{ij}}{\sum_j \tilde{C}_{ij}}$$

where d_{ij} is the distance in km between habitats *i* and *j*. This indicator shows the average distance in km at which habitat *i* can send its larvae. The source index (SI) of habitat *i* is a measure of the potential of habitat *i* to be a source of larvae for multiple sink habitats *j*. It is obtained by:

$$SI_i = n_{ji} \cdot \sum_j \tilde{C}_{ij}$$

where n_{ji} is the number of habitats *j* to which habitat *i* sends larvae. This allows us to identify habitats that can be considered as good source of larvae, since an habitat with a high SI either sends many larvae that settles, or sends larvae to a lot of different sink habitats, or both.

Another indicator we analyze in this section is the proportion of larvae that settle on habitat *j* compared to the total number of larvae released:

$$LS_j = \frac{\sum_i C_{ij}}{\sum_i S_i}$$

We also apply a community detection algorithm on our habitats network. The aim is to find sub-groups of highly connected habitats. To do so, we use Tarjan's algorithm (Tarjan 1972) with Nuutila's modifications (Nuutila and Soisalon-Soininen 1994). This method, called the strongly connected components (SCC) method, is not based on the strength of the connections between habitats but on the presence of bi-directional connections. Two habitats will be in the same community if they send larvae to each other. They can also be in the same community if the bi-directional connection is made in several steps. This allows to find groups of habitats in which genetic mixing is high.

All the analysis described here are performed on the results of the five-month simulation, but also for each of the individual spawning events to see the evolution of the connectivity through time. The duration of the larval stage changes with water temperature and is therefore not constant throughout the five months. To isolate the impact of each spawning event on the connectivity, we look at the time it took for all larvae released in one of the events to settle. We then divide the five months in seven periods, as described in Table 2.

Table 2 : Periods for which the connectivity study was performed.

Period n°	Time of spawning	Time of final settling	Duration
1	1st of May	11th of June	41 days
2	22nd of May	25th of June	34days
3	12th of June	11th of July	29 days
4	3rd of July	31st of July	28 days
5	24th of July	21st of August	28 days
6	14th of August	9th of September	26 days
7	4th of September	1st of October	27 days

We do not to perform a community study for each spawning event. We instead evaluate habitat isolation by looking at the self-recruitment index. The self-recruitment index (SR) is the proportion of larvae settling on habitat *j* that come from *j*, compared to the total amount of larvae settling on habitat *j*:

$$SR_j = \frac{\tilde{C}_{jj}}{\sum_i \tilde{C}_{ij}}$$

To compare the different spawning events, we take for each of them the average of their self-recruitment indices.

2.5. Impact of climate change

To evaluate the impacts of climate change, we run the dispersal of the larvae for three different scenarios. The first one is set in normal conditions, with temperature as modelled by SLIM and the pH at 8.075. The second scenario (called the “Extreme CC” scenario in the rest of this work) assumes a pH of 7.645 and a temperature increase of 3°C, since ocean’s temperature is thought to increase by 1-3°C by 2100, while the pH is expected to decrease by 0.14-0.43 unit (Hoegh-Guldberg et al. 2014). This second scenario should therefore be seen as a “worst case scenario”. A third intermediary scenario (called the “Mild CC” scenario) assumes a pH of 7.8 and a temperature increase of 1°C, to see the impact of milder climate change.

The impacts of climate change on the larvae depth distribution can be seen in the theoretical case presented in Figure 14. In this case, we only represent the depth variation due to the variations of w_B throughout the different larval stages. The horizontal dynamics due to the currents is therefore not taken into account. We also represent the change in depth at a point where the maximal depth is equal to the maximal depth at which the crabs can be found, to accentuate the differences between the three scenarios. For the normal scenario, we set a constant temperature of 27°C. As a consequence, the temperature of the extreme CC scenario is 30°C and the temperature for the mild CC scenario is 28°C. As a result of the decreased pH and increased temperature, the larva stays close to the ocean floor and its larval stage duration is decreased by three and six days for the mild CC and extreme CC scenario respectively.

All the indices described in the previous section are computed for the three scenarios. Since temperature changes from one scenario to another, the seven periods for the connectivity study are adapted for the two climate change scenarios. They can be found in Table 3 and Table 4.

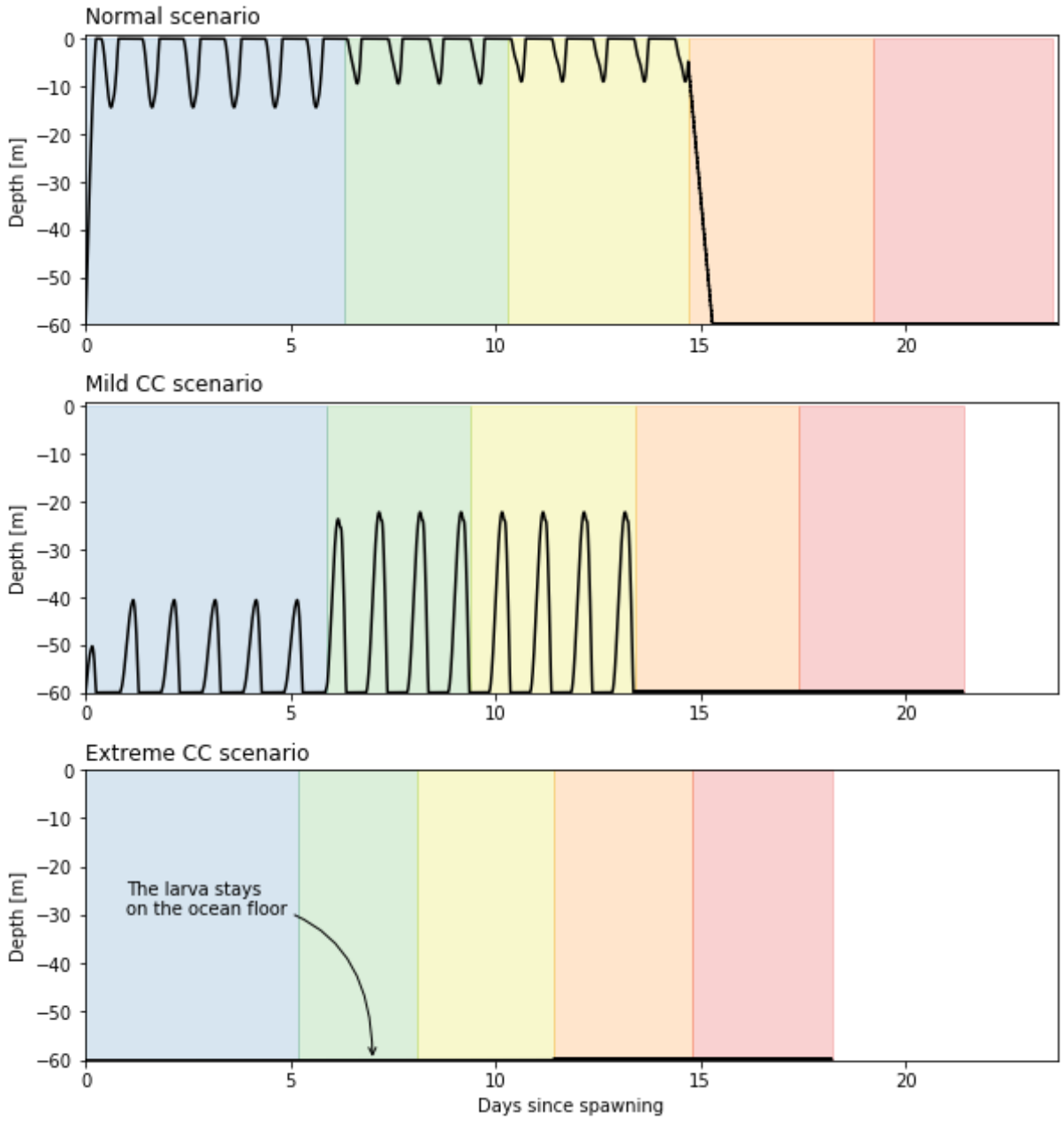

Figure 14 : Theoretical vertical movements (black line) of a stone crab larva throughout all its larval stages, according to the different scenarios presented in this work. The colors represent the duration of the different larval stages. The temperature and pH are of 27°C and 8.075 for the normal scenario, 28°C and 7.8 for the intermediary scenario and 30°C and 7.645 for the pH and T scenario.

Table 3 : Periods for which the connectivity study was performed for the extreme CC scenario.

Period n°	Time of spawning	Time of final settling	Duration
1	1st of May	2nd of June	32 days
2	22nd of May	19th of June	30 days
3	12th of June	11th of July	29 days
4	3rd of July	30th of July	27 days
5	24th of July	20th of August	27 days
6	14th of August	7th of September	24 days
7	4th of September	1st of October	27 days

Table 4 : Periods for which the connectivity study was performed for the mild CC scenario.

Period n°	Time of spawning	Time of final settling	Duration
1	1st of May	7th of June	37 days
2	22nd of May	24th of June	33 days
3	12th of June	15th of July	33 days
4	3rd of July	30th of July	27 days
5	24th of July	24th of August	31 days
6	14th of August	9th of September	26 days
7	4th of September	1st of October	27 days

3. Results

In this section, we will first present the results of the hydrodynamic model. We will then expose the results of the different connectivity studies we made for the different scenarios.

3.1. Hydrodynamic model

We validate three variables of the hydrodynamic model: the horizontal velocity, the temperature and the salinity of the water.

The horizontal current velocity simulated with SLIM 3D from May to September 2019 compares well to observations at station 42023 (Figure 15). We also compared SLIM model outputs with HYCOM's output and put them both in perspective with the wind forcing from ERA5. All these sources have been resampled to compare them at the same points in time. This is achieved by defining windows of 3 hours and taking the mean of all the values of the velocity components U and V in that window and repeating every 3 hours. SLIM's output are closer to observations than HYCOM's outputs even if the observation point is far from the coast and hence not directly influenced by the coastal topography

We can however see on the histogram of the currents direction that SLIM generates northward currents that are not observed at the station. This is not due to a single event, as we can see on the sticks plots (Figure 15) that SLIM tends to have more northward currents than what is observed. Moreover, SLIM does not fully represent the extreme southward current events that appear in the observations in June and July. This tendency to produce northward currents can also be found in the two lasts stick plots that present the horizontal velocity of the forcings.

Regarding the temperature and salinity, the comparison between SLIM's output and NOAA's observations can be found in Figure 16. Even though SLIM tends to underestimate the water temperature, it still follows the right trend. We also observe the apparition of a vertical stratification of the temperature during the simulation. The salinity outputs of SLIM appear to be relatively constant, both over time and as a function of depth. As a result, SLIM does not represents the decrease in salinity observed in June.

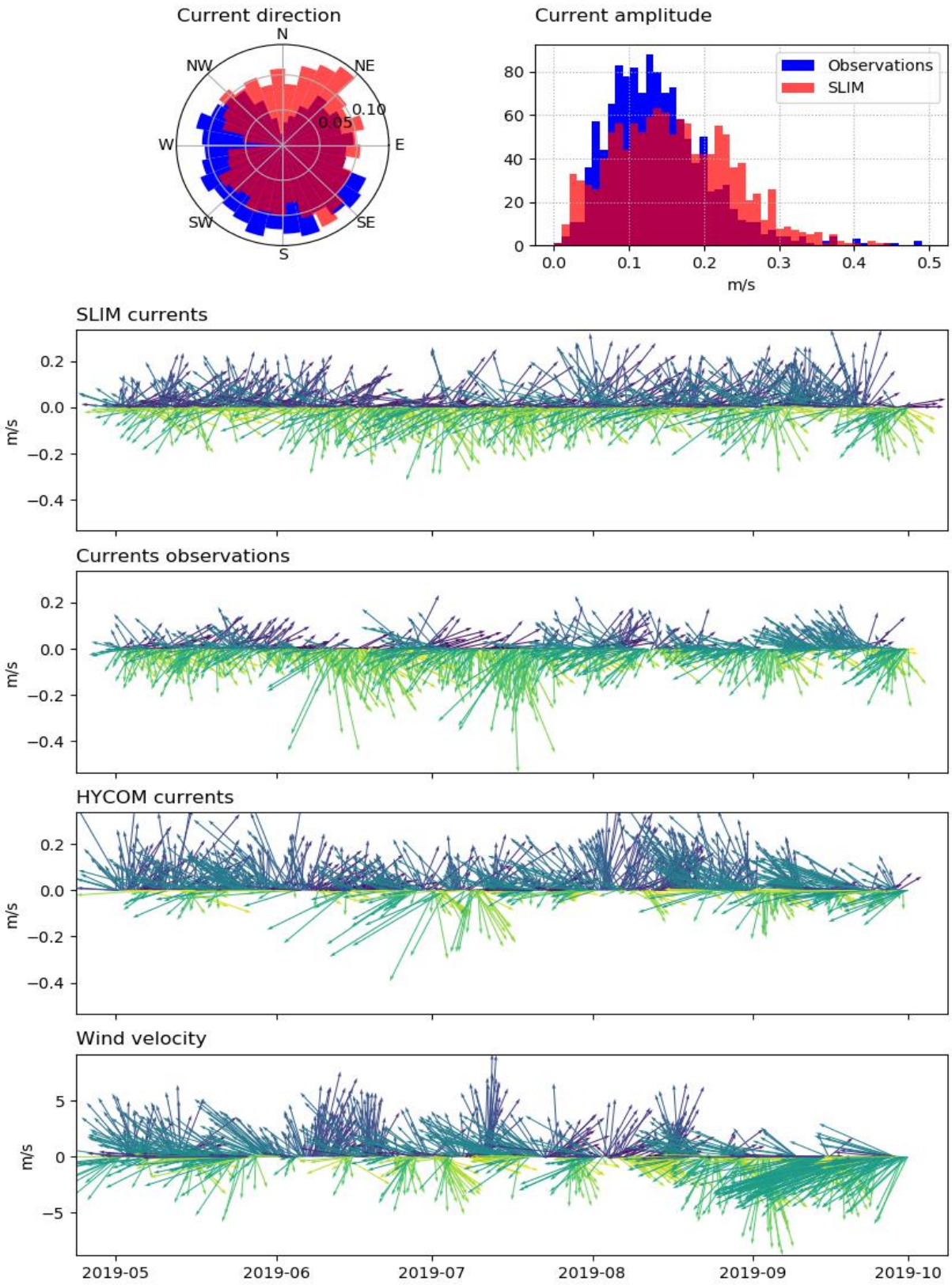

Figure 15 :Comparison of the horizontal velocity outputs of SLIM with observations from the NOAA and forcings from HYCOM and ERA5 (wind velocity) from May to September 2019. The currents are measured and modeled four meters below the surface at station 42023 (26.010° N and 83.086° W). The wind velocities are modeled 10 meters above the surface at the same coordinates. The first two graphs are histograms of the direction and amplitudes of the currents comparing SLIM with observations. The four other plots present the evolution of the horizontal velocities throughout the study period (an arrow pointing up represent a northward current). The color stresses the direction of the currents.

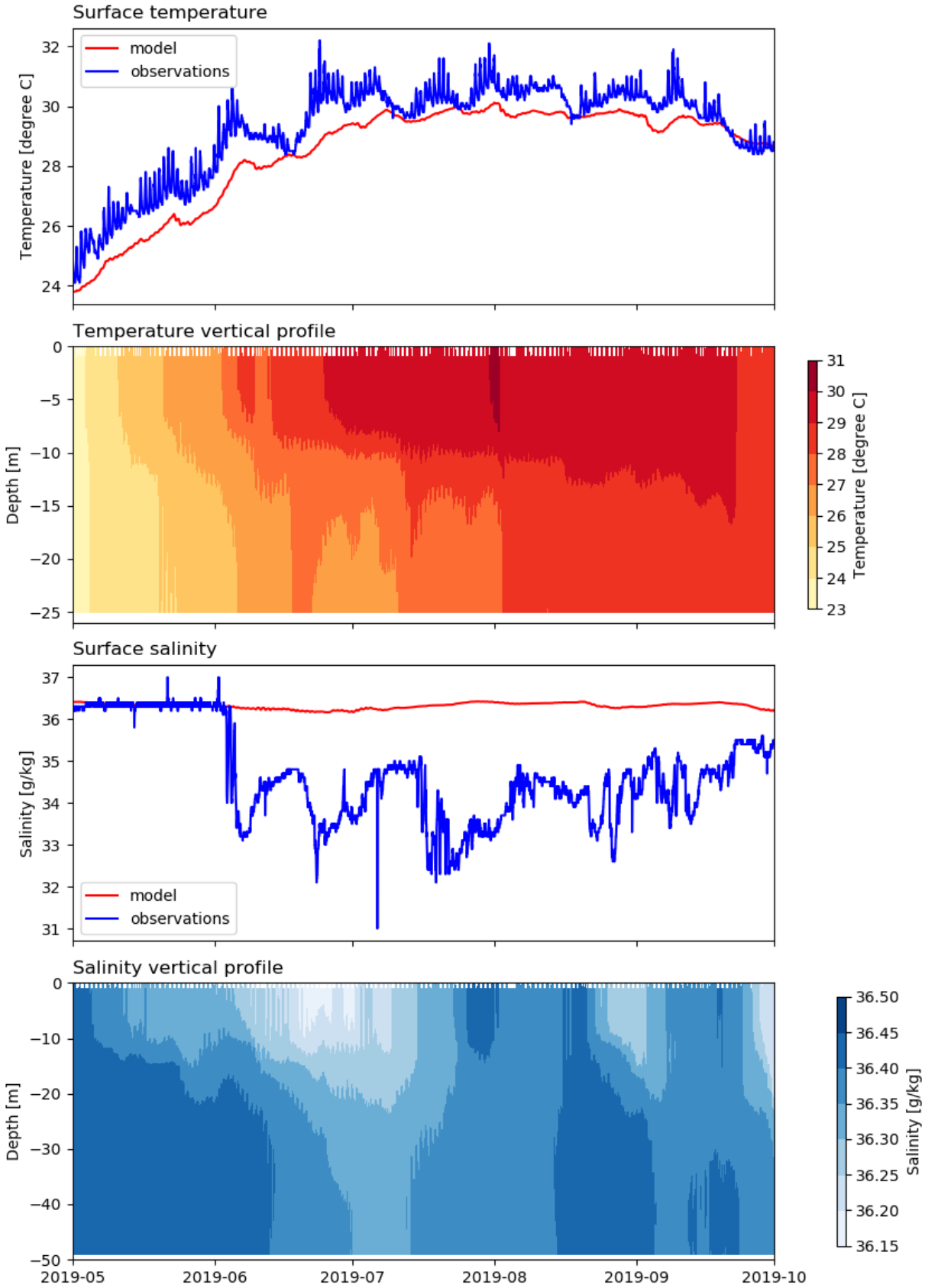

Figure 16 : Validation of temperature and salinity outputs of SLIM. First and third graphs show respectively SLIM's temperature and salinity one meter below the surface, compared with observations at the same point. The second and last graphs show the evolution of the temperature and salinity with time and depth. The point of validation for the temperature and salinity are respectively 27.173°N - 82.924°W and 27.505°N- 83.741°W.

3.2. Connectivity and climate change

The results for the connectivity studies made for the different scenarios show that climate change has an impact on the distribution of the larvae.

The proportion of total exchanges between habitats of the same zone (fishing zone or non-fishing zone) changes significantly between the normal and extreme CC scenarios (Figure 17): between habitats of the fishing zone, it decreases from almost 80% to less than 60% respectively, while between habitats in the non-fishing zone it increases from almost 20% to almost 40%. The results for the mild CC scenario are in between with a proportion total exchanges between habitats of the same zone of 70% and 20% for the exchanges between the habitats in the fishing zones and between the habitats in the non-fishing zone respectively. The proportions of exchanges happening between habitats of different zones are rather low (5% or less for all scenarios) and constant between the different scenarios.

Interestingly, the changes in the proportion of total exchanges between habitats of the same zone are mainly due to a significant increase in the number of larvae involved in the exchanges between habitats of the non-fishing zone. The proportion of the spawned larvae involved in those exchanges increases from 0.12% in the normal scenario, to 0.17% in the mild CC scenario and 0.34% in the extreme CC scenario. The change in the number of larvae involved in the exchanges between the habitats of the fishing zone is less consequent. The proportion of spawned larvae involved in those exchanges rises from 0.52% in the normal scenario to 0.6% in the mild CC scenarios before decreasing to 0.57% in the extreme CC scenario.

The distance between the spawning habitat and the habitat on which the larvae settle tends to decrease with the intensity of climate change (Figure 18). The median distance traveled by a larva in the normal scenario is 25.2 km, while in the mild CC scenario it is 18.5 km and in the extreme CC scenario it is 10.8 km. Likewise, the maximal distance traveled by a larva is higher for the normal scenario (124 km) than in the mild CC (106 km) scenario. The maximal distance in the extreme CC scenario is higher than the other two (132 km), but we can see on the map that it is due a single habitat in the south of the domain that sent its larvae far away. For all three scenarios, the habitats that produce the larvae that travels the most are the ones situated farther away from the mainland, on the eastern and southern part of the domain.

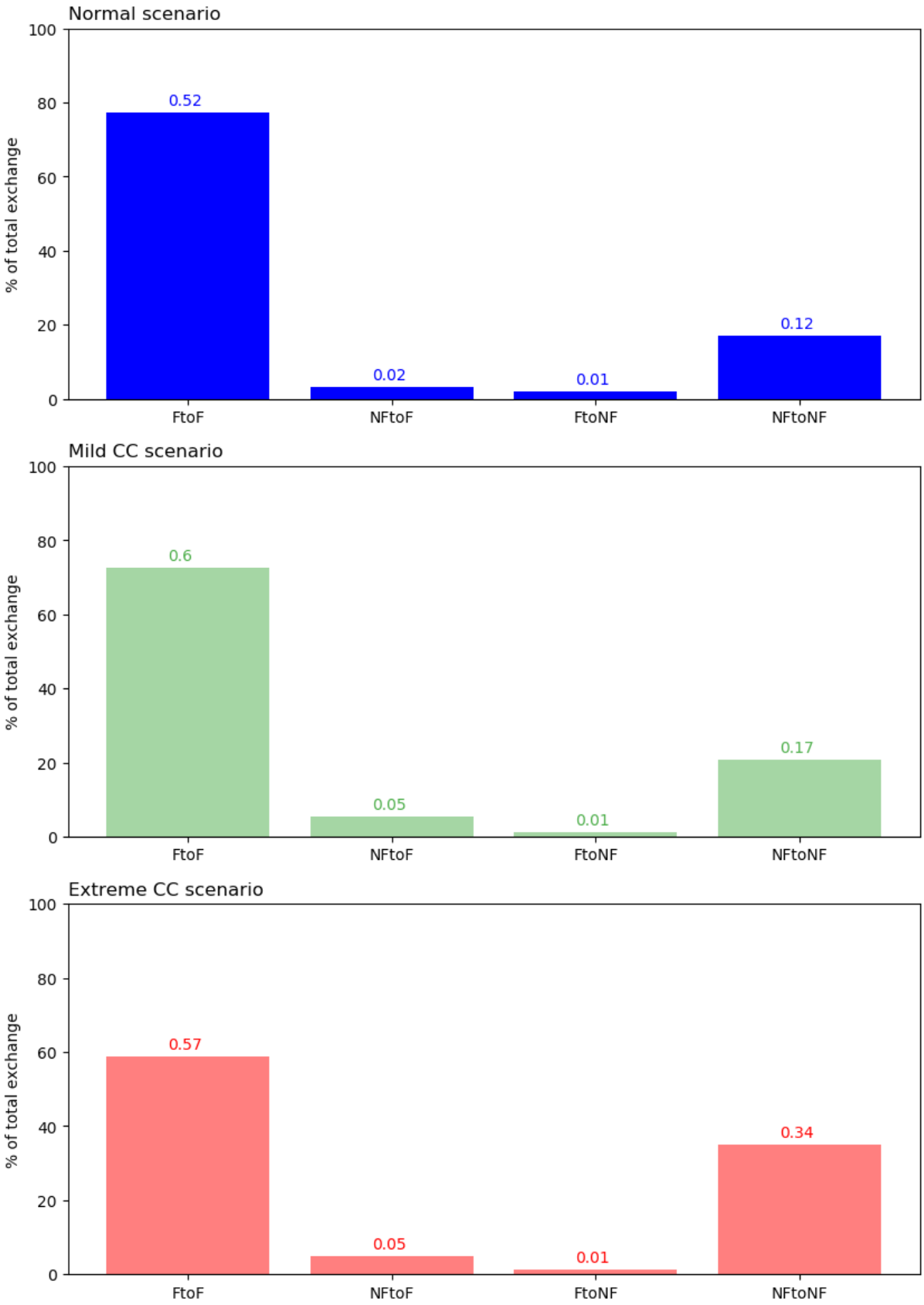

Figure 17 : Proportion of all the exchanges that happened between habitats in the fishing zone (FtoF), between habitat from the non-fishing zone and the fishing zone (NFtoF), between the habitat of the fishing zone and the non-fishing zone (FtoNF) and between the habitats of the non-fishing zone (NFtoNF). The numbers above the bars indicates the percentage of the spawned larvae that are involved in those exchanges. Each graph represents a different scenario.

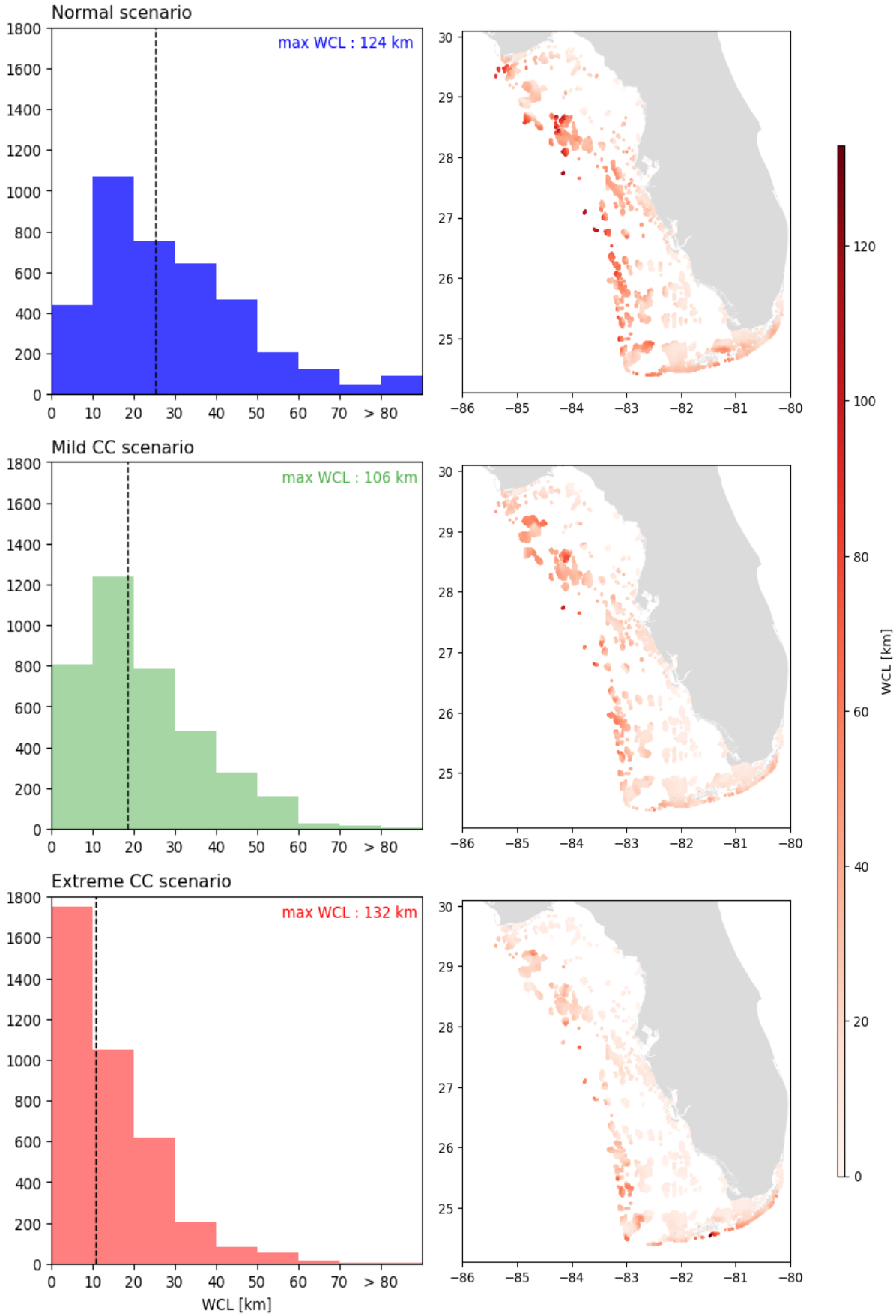

Figure 18 : WCL histogram and map for each scenario. The maximum WCL for each scenario is written on the top right corner of the corresponding histogram. The vertical dotted line on the histograms represents the median WCL.

The source index values distributions are relatively similar for the three scenarios (Figure 19). The median source index for the normal, mild CC and extreme CC scenarios are 0.2, 0.24 and 0.24, respectively. There are however more habitats with a high (> 3) source index in the mild CC scenario (144 habitats), followed by the normal scenario (109 habitats) and the extreme CC scenario (0 habitat). The maximal source index is found in the normal scenario (6.71), followed by the mild CC scenario (5.92) then the extreme CC scenario (2.53). The habitats around the Florida Keys are an important source of larvae for the normal and mild CC scenarios, but their source index is lower for the extreme CC scenario. The source index of the northern and deeper habitats increases in scenarios subjected to climate change. All three scenarios have many habitats with a low (< 0.5) source index.

The proportion of the spawned larvae that settles increases with the intensity of climate change (Figure 20). For the normal scenario, only 0.67% of the spawned larvae settle on a new habitat. This number increases to 0.83% for the mild CC scenario and 0.97% for the extreme CC scenario. This increase is visible on the maps, as more larvae settles in the north and away from the mainland as climate change intensifies. There seems to be an important number of larvae that settles around the Florida Keys in the normal and mild CC scenarios, but it is less marked in the extreme CC scenario. Very few larvae settled in the northeastern part of the domain for all three scenarios.

The number of communities found with the SCC method increases with the intensity of climate change (Figure 21). The normal scenario has 14 communities, while the intermediate and extreme CC scenarios have 17 and 52 communities, respectively. As a result, the size of the average size of the community also decreases with the intensity of climate change. The community average size for the normal, mild CC and extreme CC scenario are 375 habitats, 174 habitats and 101 habitats, respectively. Another interesting thing to note is that for the mild CC scenario there is a large area without any community on the north part of the domain. This means that none of the habitats in that zone are involved in a mutual exchange of larvae with other habitats.

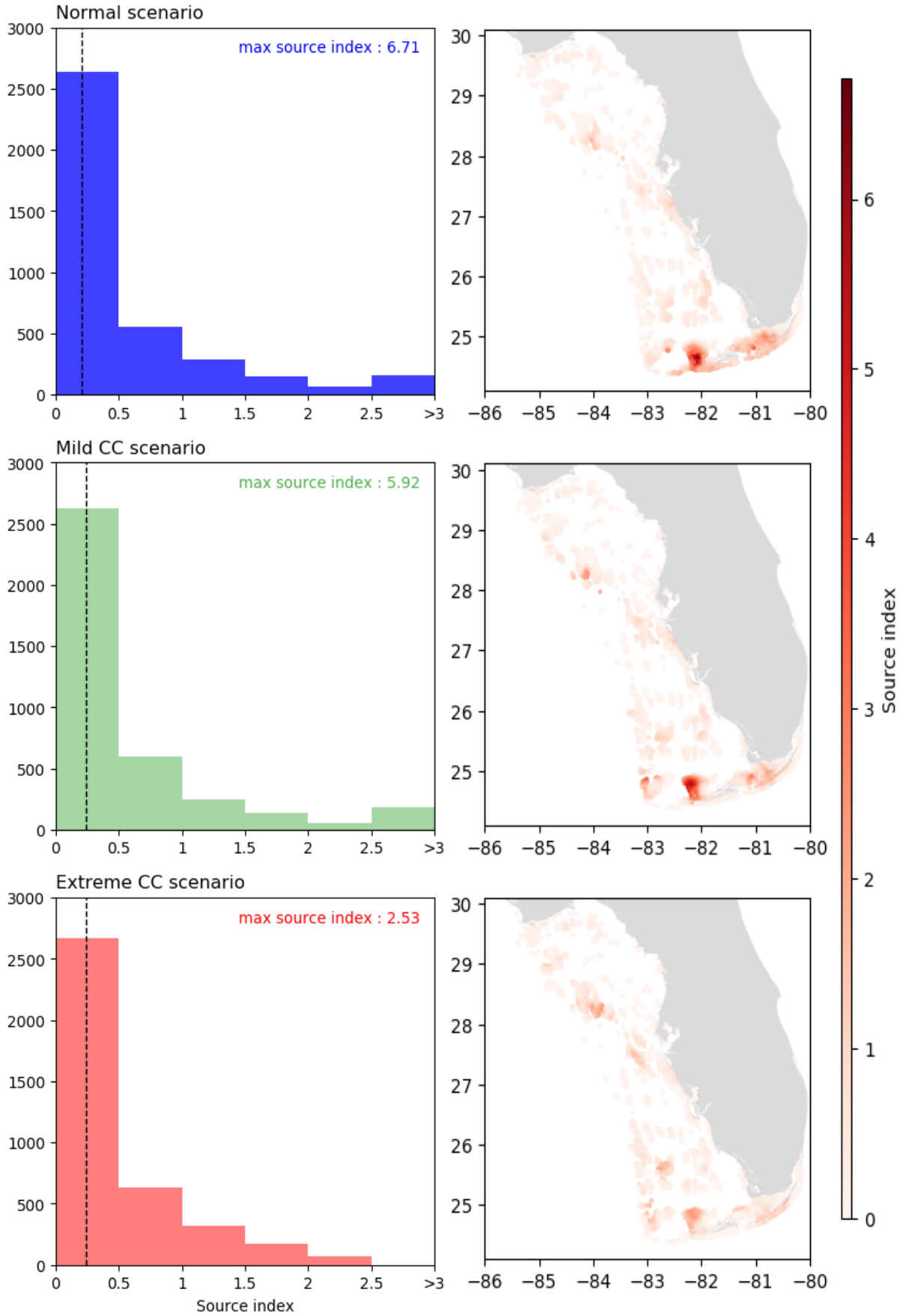

Figure 19 : Histogram and map of the source index for each of the scenario. The maximum source index for each scenario is written on the top right corner of the corresponding histogram. The vertical dotted line on the histograms represents the median source index.

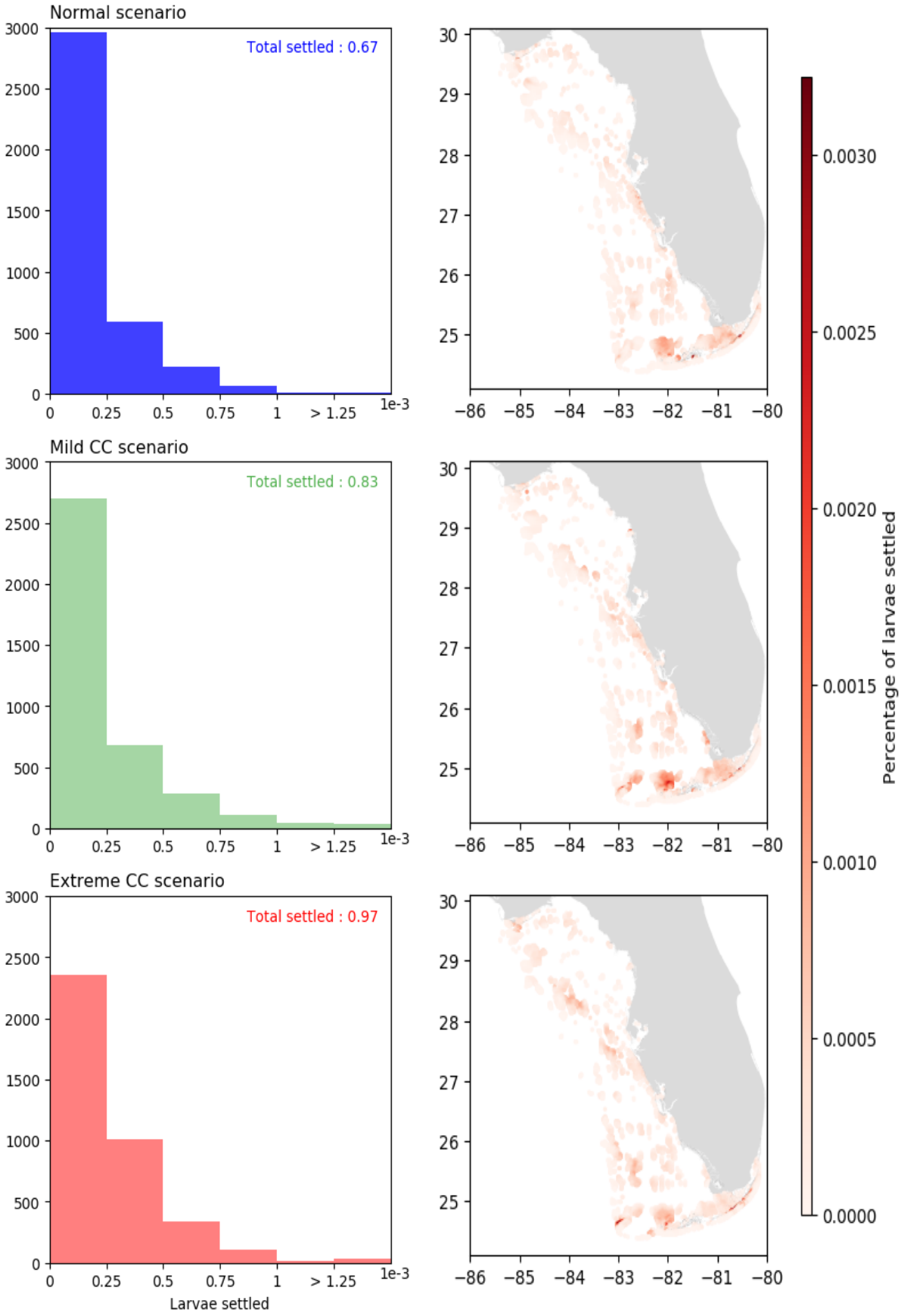

Figure 20 : Histogram and map of the proportion of spawned larvae that settles for each of the scenario. The total percentage of spawned larvae that settles for each scenario is written on the top right corner of the corresponding histogram

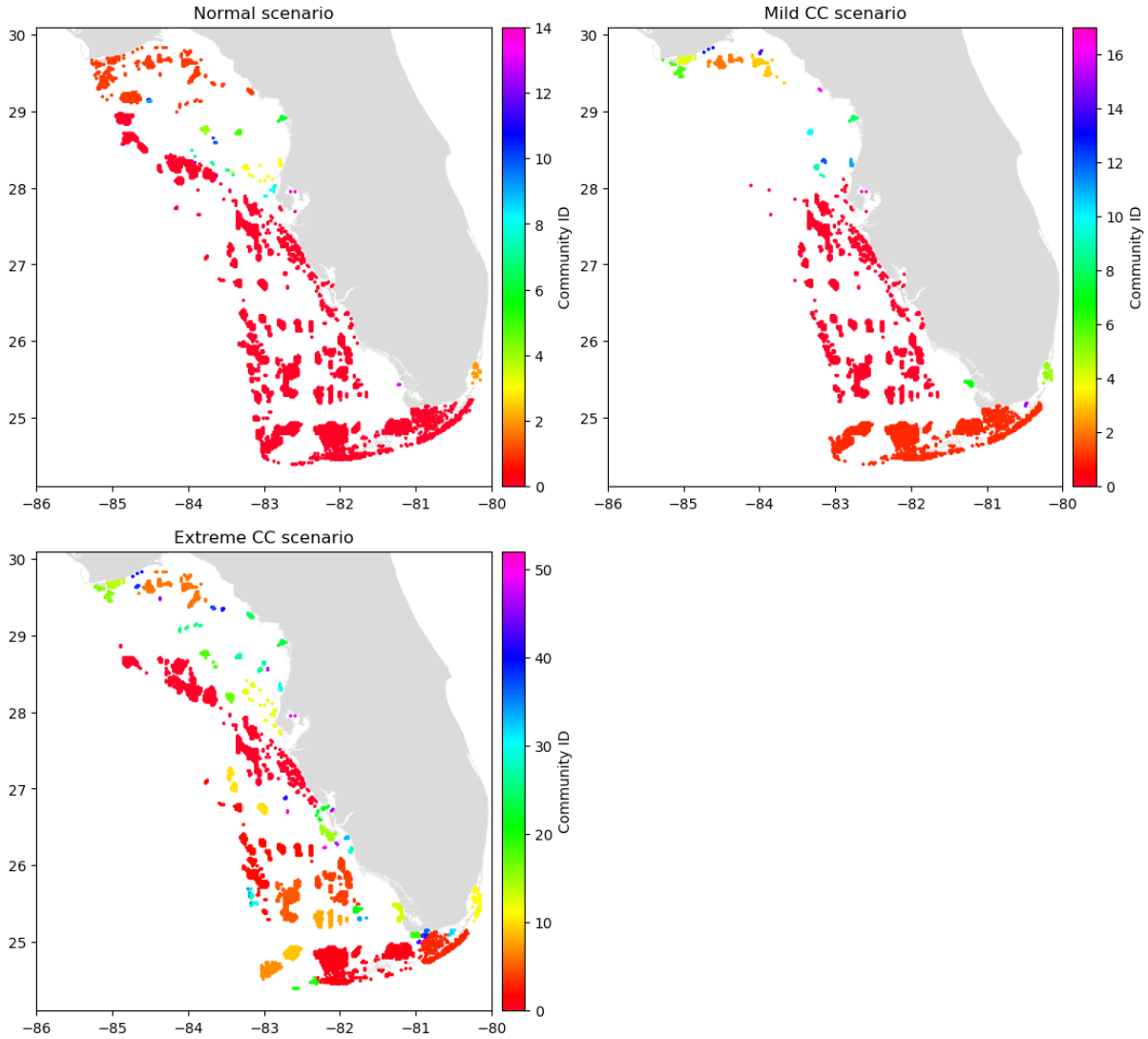

Figure 21 : Maps of communities obtained with the SCC method for each of the scenario.

Concerning the evolution of WCL and self-recruitment throughout the different spawning events, there is no clear trend that emerges for the different scenarios taken individually (Figure 22). Unsurprisingly, the WCL and self-recruitment graphs are opposed to one another. The WCL of the normal scenario is always higher than the one of the mild CC scenario, which is generally higher than the extreme CC scenario. For the self-recruitment it's the extreme CC scenario that is higher than the other two, followed by the mild CC then the normal scenario. For both of these two indices, there is a swap on the last spawning events between the normal scenario and the mild CC scenario, where the WCL and self-recruitment of the mild CC scenario pass respectively above and below those of the normal scenario.

The evolution of the proportion of the spawned larvae that settles is different for the three scenarios. For the normal scenario, the proportion seems to increase throughout the spawning period. The proportion of settled larvae for the mild CC scenario increases up until the 5th spawning event, then decreases for the last two spawning events. The proportion of settled larvae in the extreme CC scenario seems relatively constant up until the 5th spawning

events, after which it decreases. Each scenario is at some point of the study period the one with highest proportion of spawned larvae that settles. The extreme CC scenario has the highest proportion of settled larvae for the 4 firsts events, the mild CC scenario has the highest proportion for the 5th spawning event, and the normal scenario has the highest proportion for the last two events.

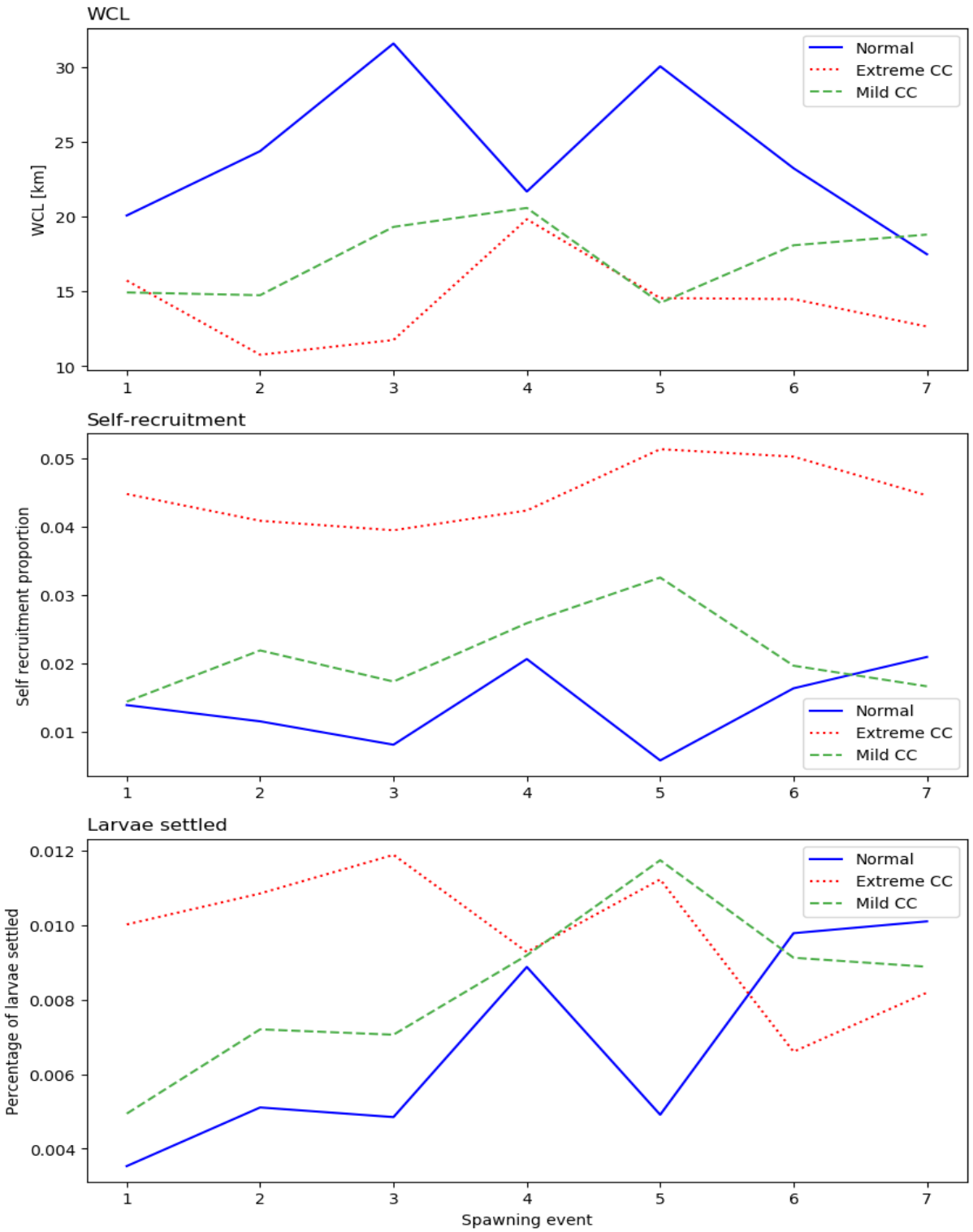

Figure 22 : Evolution of the WCL, self-recruitment and proportion of spawned larvae that settle throughout the seven spawning events for the three scenarios.

4. Discussion

In this section we will discuss the validation of SLIM3D's results and the implications of the results of the connectivity study.

4.1. Hydrodynamic validation

The aim of this part is to evaluate if SLIM3D is able to effectively reproduce the physical processes observed on the WFS during the summer of 2019.

As explained in the previous section, the temperature modelled by SLIM seems to follow the right trend, even though it is slightly lower than the observed temperature (Figure 16). In addition, we can observe a transition from an horizontal to a vertical stratification of the temperature as the summer goes on, which is typical of mid-latitude continental shelves and has been observed on the WFS (He and Weisberg 2002, 2003).

Concerning the horizontal velocity of the currents (Figure 15), the apparition of northward currents and the reduced number of southward currents compared to observations are probably due to HYCOM forcing. The results still follow relatively well the observations. Moreover, SLIM seems to catch the southward currents better than HYCOM.

An interesting fact is that neither SLIM nor the observations seem to follow the northwestward trend observed in summer by Liu and Weisberg (2012). Looking at observations from different years at the same point and period (Figure 23), we can see that there is no clear trend that emerges between the different summers. This might be due to the fact that the point of validation is situated near the 50m isobath. Liu and Weisberg (2012) indeed observed that seasonality of the currents is less pronounced from the 50m isobath and deeper.

The constancy of the salinity value in the SLIM results (Figure 16) is more than likely due to poor results from HYCOM regarding the salinity. Indeed, we use HYCOM's salinity results to force SLIM both at the surface and on the open boundaries. As a result, we have an overestimation of the salinity of about 2 g/kg. However, salinity is only involved in one of the processes of larval dispersal, namely the survival rate of stage 1 larvae. We therefore chose to overlook this overestimation. It is however important to note that mortality might be slightly overestimated as a result.

In conclusion, we consider that SLIM represents the observed physical processes well enough to be used for larval dispersal.

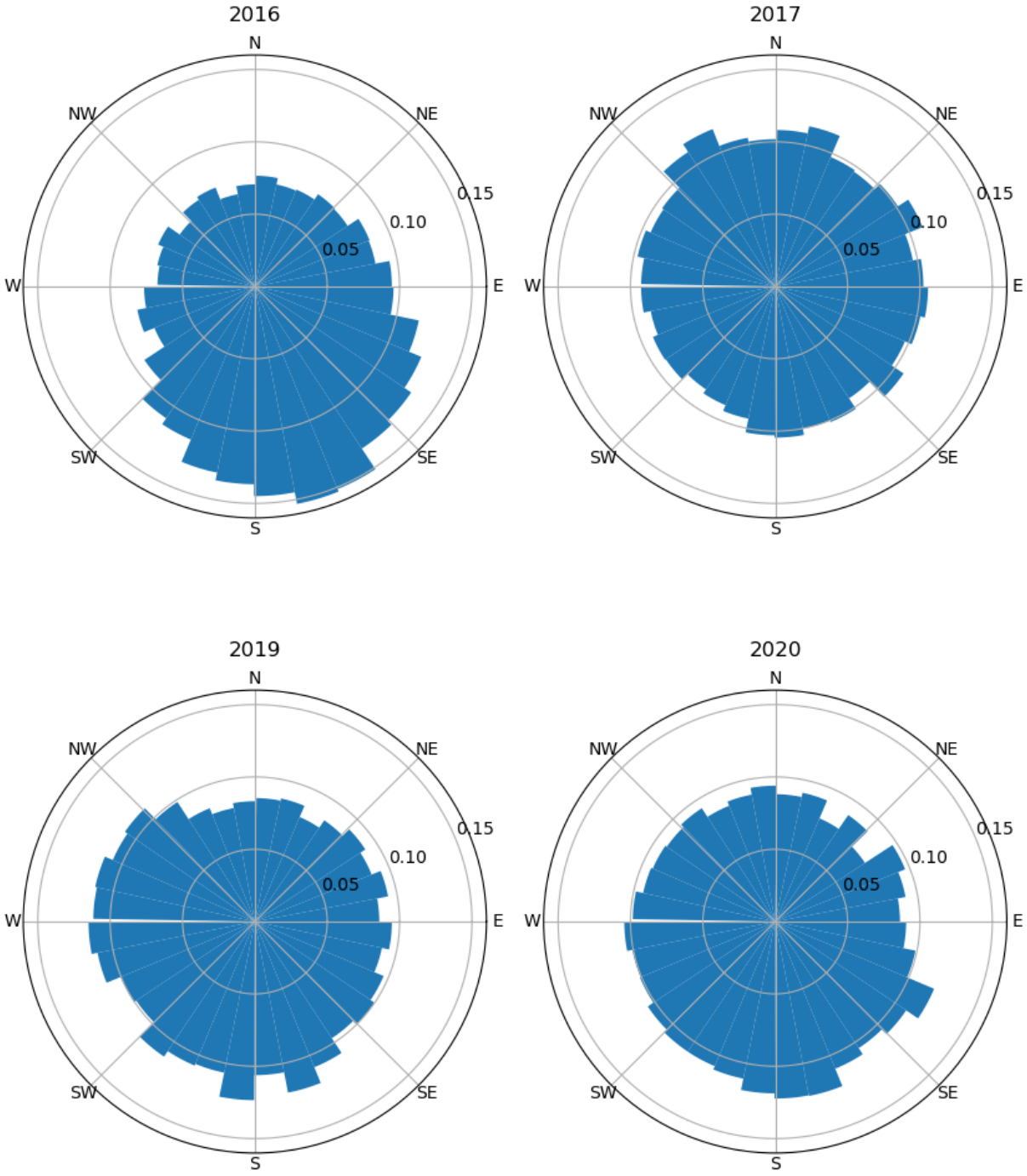

Figure 23: Comparison of the repartition of currents' direction for the summer of four different years (2016, 2017, 2019 and 2020), from the 1st of May to the 1st of October. The data comes from observations made by the NOAA at 26.010° N and 83.086° W (National Oceanic and Atmospheric Administration 2021). The year 2018 was not used since the measurements only began in mid-June.

4.2. Larval dispersal and climate change

The results of our connectivity study on all three scenarios allowed us to better understand the way stone crab's larvae disperse and to evaluate the potential for the non-fishing zone habitats to be a source of larvae for the fishing zone habitats. It also highlighted potential effect of climate change on larval dispersal: in the years to come, we expect a shift in the spatial distribution of the crab, an increase in the number of larvae settling and an important decrease in the size of the communities present in the WFS.

By looking at the source index and settlement maps of the normal scenario (Figure 19 and Figure 20) we can observe that the larvae tend to follow a north-northwest dispersal pathway. This is consistent with the northwestward average current observed by Liu and Weisberg (2012) during summer. Temperature is a major factor influencing the fraction of larvae that successfully settles. This is mainly due to the mortality rate being a function of temperature. In the normal scenario, the number of settlers is higher in southern and shallow areas, because the temperature of the water in the north and in deeper water is too low to allow much settlement for the first spawning event. With a small increase in temperature, like in the mild CC scenario, the proportion of spawned larvae that settles increases in the north and in deeper water, but also in the south. As a consequence, the number of larvae settled stays higher in the south of the domain than in the north. When the temperature increase is larger, like in the extreme CC scenario, the temperature exceeds the larvae temperature optimum in the south, decreasing the survival rate of the larvae in that part of the domain. As a result, the proportion of spawned larvae that settles does not really increase in the south part of the domain compared to the normal scenario, but we can see an increase in the north and in deeper area. We conclude that climate change could trigger a northward and/or deeper water shift in the spatial distribution of the stone crab larvae on the WFS. This kind of shift to deeper or higher latitude water due to climate change has been observed for several marine species (Fujiwara et al. 2019; Mieszkowska et al. 2006), as well as other brachyuran crabs (Murphy 2020).

The hypothesis that the habitats in the non-fishing zone could serve as a source of larvae for the habitat in the fishing zone is ruled out by the small number of exchanges happening between the two types of habitats in all three scenarios. In a context of a decreasing number of catches, it is therefore important to concentrate any restauration actions, should they be needed, on the habitats of the fishing zone. The habitats around the Florida Keys especially seem to be a good source of larvae in all three scenarios, even though their source index decreases in the extreme CC scenario.

One of the main impacts of climate change on the stone crab population of the WFS is the increase of the number of settling larvae. This increase is most likely due to the increase of water temperature that increases larval survival rates during most of the simulation. Émond,

Sainte-Marie, and Bêty (2020) observed this kind of climate change induced evolution of the abundance of other brachyuran crabs. This is however not necessarily good news for the stone crab fishing industry. Indeed, the number of larvae that settle increases mainly outside the fishing zone, while the proportion of spawned larvae settling in the fishing zone only slightly increases. This difference is probably due to the difference in temperature between the two zones. The non-fishing zone is set in deeper water which means that the temperature near the habitats is going to increase more slowly than in shallower water, where the temperature is more uniform. As a consequence, it takes more time for the temperature around the habitat in the non-fishing zone to exceed the temperature optimum of the larvae. The larvae that stay near those habitats can therefore benefit of the temperature increase over a longer part of the study period. Since there are very few exchanges of larvae between the fishing and non-fishing zones, this increase of settled larvae would not be beneficial to the fishery. Moreover, we did not take into account the increase in mortality caused by decreasing pH (Gravinese et al. 2018). We also did not take into account the fact that a decrease in pH induce an increase in the time needed by the eggs to hatch and a decrease in the number of eggs that hatches (Gravinese 2017). This leads us to think that the number of stone crabs in the fishing zone could actually decrease due to climate change.

Another impact of climate change according to our results is the decrease of the WCL that leads to an increase in self-recruitment and smaller communities. This is most likely due to a combination of two factors: the downward shift of the vertical distribution in the water column due to a decrease in pH and the shorter larval stage duration due to an increase in temperature. Both the lower position and shorter larval stage duration have already proven to reduce larval dispersion of several marine species (North et al. 2008; Shanks, Grantham, and Carr 2003; Sundelöf and Jonsson 2012). This could be problematic since populations with smaller communities are less resilient than populations with larger ones. Species that have high dispersal capabilities and form big communities are indeed less vulnerable to sudden changes in external conditions and sickness thanks to higher genetic diversity and the potential of local recovery through larval transport (Hastings and Botsford 2003; Jones, Srinivasan, and Almany 2007).

The last impact that we identified in our study is the possible modification of the spawning period. We see significant decrease of the number of settled larvae for the 6th and 7th spawning events for both climate change scenarios. This lower number of larvae that settle for the two last spawning event is most likely due to the temperature. Indeed, the last two spawning events begin on the 14th of August and 4th of September respectively, when the water temperature is the warmest. With an increased temperature, we could then expect the spawning season to shift and begin earlier in the season. The high proportion of larvae that settled during the first spawning event support that theory. Different studies observed this earlier phenology due to the effects of climate change on a variety of marine species (Przeslawski et al. 2008), including other brachyuran crabs (Émond et al. 2020). Another

possibility of modification in the spawning period would be to have another peak of spawning in October, when the water temperature is not too high for the larvae. This theory is supported by the fact that spawning can happen all year long in the south if the temperature is right (Krimsky et al. 2009; Lindberg and Marshall 1984).

4.3. Study limitations

Given that this thesis is the first to attempt to model the dispersion of *M. mercenaria*, and given the assumptions that we had to make, this study has obviously some limitations. Here we discuss the most important assumptions in order to highlight which aspects of our study could be improved in the future.

The main limitation for this work was the lack of easily usable data on the stone crab. Many assumptions were made to represent the crabs behavior. These include the description of the vertical larval dynamics and the location of crabs habitats. Even though those hypotheses were deemed reasonable, they probably introduce some kind of bias. Two main studies could be conducted to help improve the inputs of this model. The first one would be to conduct vertically stratified plankton surveys, that could be used to restrict the experiment-based vertical velocities by the depth distribution of the larvae, like in Peliz et al. (2007). The second useful input would be to better map stone crabs habitat. This could be done in different ways, either by field observations or by using backtracking to identify the source habitat of observed crabs, like in Criales et al. (2019).

Another limitation of our model comes from SLIM3D's salinity results. As explained earlier, the lack of variability in SLIM's salinity leads to overestimate the actual salinity values. As a consequence, the mortality rate of stage 1 larvae is probably overestimated as well. A better estimation of the salinity, through maybe the use of a more accurate forcing, could increase the quality of the model and predictions.

Because of the time constraint and the time required to run simulations, we had to limit the number of particles being released above the habitats to a density of 1 particle/km^2. Increasing the number of particles released could allow to draw conclusions that are more statistically robust.

To simplify the development of the model we chose not use the impact of pH on the survival rate and hatching. As a result, the number of crabs settling in the climate change scenarios are probably slightly overestimated. Taking those into account could therefore increase the precision of the predictions.

Another way to improve the predictions would be to integrate the spatial heterogeneity of the pH, pH decrease and temperature increase over the domain. In our study, we used a fixed value of pH over the entire domain and also decreased (increased) the pH (temperature) of a fixed value. However, pH changes both horizontally over the WFS (NOAA Ocean

Acidification Program 2020) and with depth (Byrne et al. 2010). Likewise, the future pH decrease and temperature increase are probably not going to be spatially homogeneous.

In this study, we chose not to separate the impact of pH decrease and temperature increase between different scenarios. This means that we cannot clearly differentiate the effect that each of those changes has individually. Since pH decrease is not only due to climate change, but also to the increase of nutrients in coastal waters, it could be interesting to do separate scenarios for ocean acidification and ocean warming to isolate their individual effects.

We also chose to use the same hydrodynamics for all three scenarios, thus assuming that the currents will not be significantly influenced by climate change. This approach is supported by the observations made by Figueiredo et al. (2021) on coral larvae in Australia. They evaluated that the changes in circulation due to climate change will only have a small impact on larval dispersal, compared to the biological changes induced by climate change. Morey et al. (2017) seems however to think that not only will the currents on the WFS change due to climate change, but that those changes will impact larval dispersal of several species. It could therefore be interesting to evaluate the impacts that potential changes in the circulation could have on the dispersal of stone crab larvae.

The last limitation we wanted to address here is the fact that we did not consider what happens after the settlement. We implicitly assumed that a larva that settles on one habitat stays there for its entire life. This is however not necessarily the case. The habitats preferred by juveniles crabs are not necessarily the same as those preferred by adult crabs (Krimsky and Epifanio 2008). Separating the settlement habitats and the habitats on which adult stone crabs can be found would be an additional way to improve this study.

For all these reasons, the results of this study should be used as qualitative indicators, rather than quantitative ones.

4.4. Potential applications

At the end of this work, we have a variety of results that can be used for diverse applications.

The first interesting result is that we successfully managed to reproduce the hydrodynamics of the WFS. SLIM3D allowed us to have a good representation of both the temperature and the currents. The modelled currents are closer to observations than HYCOM's. There is therefore an interest in using a higher resolution model on the continental shelf as it allows to have more accurate results near the coast but also offshore. Our model could therefore be used for future studies in the region.

Our work could also serve as a reference for other studies aiming to model the dispersion of brachyuran crabs. Brachyuran crabs are found all around the world, in almost all coastal habitats, and some species are commercially important (Azra et al. 2020). In this work we introduced several new elements compared to other dispersal models of brachyuran crabs, like the sinusoidal response to light (more realistic than a binary up and down vertical swimming behavior) or the pH-dependent vertical velocity component that allowed to evaluate the impacts of ocean acidification on the stone crabs distribution. Since all brachyuran crabs respond to external stimuli like hydrostatic pressure and light (Epifanio and Cohen 2016), our approach could be used to model their dispersion.

As the first model to evaluate its dispersion of *M. mercenaria*, this work could help local authorities to understand the mechanisms behind it and to take actions regarding the fishery management. The different scenarios and conclusions that we were able to draw from their results could also be used to help in the planning of the stone crab fishery of tomorrow.

Finally, this work highlights the fact that more studies need to be done to fully understand *M. mercenaria* and its behavior.

5. Conclusion

The aim of this study was to evaluate the impact of climate change on the dispersion of stone crab larvae on the WFS by the mean of a biophysical model. Ocean acidification and ocean warming are the two changes induced by the increasing atmospheric CO_2 concentration that threaten the most marine species. The stone crab is one of those species that are going to be impacted by those changes. Since stone crabs are the basis of an important commercial fishery in Florida, it is important to understand the impacts that climate change could have on their distribution. Additionally, we tried to evaluate the potential of stone crabs habitats in the non-fishing zone to serve as source of larvae for the fishing zone.

The first step to model larval dispersal was to simulate the 3D hydrodynamic of the WFS for the summer of 2019. To do so, we used the 3D version of SLIM. This ocean model uses unstructured mesh which allows us to increase the resolution locally and explicitly reproduce small-scale processes that influence larval dispersal. The resulting hydrodynamics was then coupled with SLIM's LPT to model the dispersion of the larvae. We implemented stone crabs larvae vertical movements based on experimental data. We then conducted a connectivity study, based on the CM output of the dispersal model. The last part of this study consisted in the evaluation of the impacts of climate change on the different connectivity index by the mean of different scenario: one normal scenario, using the water temperature and pH of 2019, one mild climate change scenario, with a temperature increased by 1°C and a pH decreased of 0.275, and one extreme climate change scenario, with a temperature increased by 3°C and a pH decreased by 0.43.

This approach allowed us to answer to the two questions that we identified at the beginning of this study:

- ***What will be the impacts of climate change on the dispersion of stone crab larvae on the West Florida Shelf?***

We managed to identify several impacts that climate change could have on stone crab distribution in the future. The first thing to know is that even though the distribution of the larvae is mainly driven by the hydrodynamics, their settlement areas are restricted by the temperature due to the related mortality rates. A consequence of the rising ocean temperature could be a shift in the spatial distribution of the crabs to deeper or northerner waters. The second impact would be the increase in the proportion of larvae that settles. This increase would however not benefit the fishery since it would mainly occur in the non-fishing zone. Climate change are also going to affect the distance at which the larvae can travel, by causing a lower distribution of the larvae in the water column and shortening the larval stage duration. As a result, self-recruitment is going to increase and the size of the communities will decrease, which could negatively affect the resilience of the stone crab population. The last

impact we identified is the possibility of a shift in the spawning period, due to higher temperature.

- ***Can the habitats in the non-fishing zone serve as a source of larvae for the habitats in the fishing zone?***

Our results indicate that the exchanges between the habitats of the fishing and non-fishing zones are very limited. We therefore reject the hypothesis that the habitats of the non-fishing zone could serve as a source of larvae for the habitats in the fishing zone. This means that eventual restorations actions aiming at the increase of the landings should concentrate on the habitats in the fishing zone. The habitats around the Florida Keys in particular seem to be a good source of larvae.

Our study was the first of its kind on the stone crab and could therefore be improved. The best way to improve future studies would be to carry out more studies on the stone crabs. Additional data, notably on the vertical distribution of the different larval stages in the water column and on the location of crabs habitats, could improve the precision of the previsions. Another area of improvement would be to find a model more accurate than HYCOM to force the salinity. The predictions could be made more statistically robust by increasing the number of particles released by km^2. Taking into account the influence of pH on the survival rate and the spatial heterogeneity of pH, pH decrease and temperature increase could improve the precisions of the results. Further studies could also try to evaluate the individual impacts of pH decrease and temperature increase, as well as those of predicted changes in the hydrodynamics of the WFS. Finally, looking at what happens after the settlement could give more interesting results for the fishing industry.

This work also has multiple applications. The good results obtained for the hydrodynamic model show that SLIM could be used for studies to come in the region. The results of this work could help local authorities to better understand *M. mercenaria* and to take actions regarding the fishery management and its future considering the upcoming changes in the ocean conditions. Moreover, this model of stone crab dispersal could be used in the future as a base for other crab dispersal models, as other brachyuran crabs tend to have similar behavior. This work also highlights the fact that more studies need to be done on *M. mercenaria* to fully understand its behavior.

As a conclusion of this work, we can say that climate change is going to impact the distribution of the stone crabs and its fishery. To what extent these changes are going to have an impact mainly depends on our efforts and willingness to limit our emissions.

References

Androulidakis, Y. S., V. H. Kourafalou, and M. Le Hénaff. 2014. 'Influence of Frontal Cyclone Evolution on the 2009 (Ekman) and 2010 (Franklin) Loop Current Eddy Detachment Events'. *Ocean Science* 10(6):947–65.

Azra, Mohamad N., Mohd Amran Aaqillah-Amr, Mhd Ikhwanuddin, Hongyu Ma, Khor Waiho, Antonio Ostrensky, Camila Prestes dos Santos Tavares, and Ambok Bolong Abol-Munafi. 2020. 'Effects of Climate-Induced Water Temperature Changes on the Life History of Brachyuran Crabs'. *Reviews in Aquaculture* 12(2):1211–16. doi: https://doi.org/10.1111/raq.12380.

Banas, Neil S., P. Sean McDonald, and David A. Armstrong. 2009. 'Green Crab Larval Retention in Willapa Bay, Washington: An Intensive Lagrangian Modeling Approach'. *Estuaries and Coasts* 32(5):893–905.

Beck, Michael W. 1995. 'Size-Specific Shelter Limitation in Stone Crabs: A Test of The Demographic Bottleneck Hypothesis'. *Ecology* 76(3):968–80.

Bert, Theresa M., Richard E. Warner, and Lorin D. Kessler. 1978. 'The Biology and Florida Fishery of the Stone Crab, Menippe Mercenaria (Say), with Emphasis on Southwest Florida'.

Binford, Raymond. 1913. 'The Germ-Cells and the Process of Fertilization in the Crab, Menippe Mercenaria'. *Journal of Morphology* 24(2):147–201.

Brown, Susan D., Theresa M. Bert, Wendy A. Tweedale, Joseph J. Torres, and William J. Lindberg. 1992. 'The Effects of Temperature and Salinity on Survival and Development of Early Life Stage Florida Stone Crabs Menippe Mercenaria (Say)'. *Journal of Experimental Marine Biology and Ecology* 157(1):115–36.

Byrne, Robert H., Sabine Mecking, Richard A. Feely, and Xuewu Liu. 2010. 'Direct Observations of Basin-Wide Acidification of the North Pacific Ocean'. *Geophysical Research Letters* 37(2).

Ceballos-Osuna, Lina, Hayley A. Carter, Nathan A. Miller, and Jonathon H. Stillman. 2013. 'Effects of Ocean Acidification on Early Life-History Stages of the Intertidal Porcelain Crab Petrolisthes Cinctipes'. *Journal of Experimental Biology* 216(8):1405–11.

Cowen, Robert K., and Su Sponaugle. 2009. 'Larval Dispersal and Marine Population Connectivity'. *Annual Review of Marine Science* 1(1):443–66.

Criales, Maria M., Laurent Cherubin, R. Gandy, Lysel Garavelli, Mohamed Ghannami, and C. Crowley. 2019. 'Blue Crab Larval Dispersal Highlights Population Connectivity and Implications for Fishery Management'. *Marine Ecology Progress Series* 625.

Critchell, Kay, and Jonathan Lambrechts. 2016. 'Modelling Accumulation of Marine Plastics in the Coastal Zone; What Are the Dominant Physical Processes?' *Estuarine, Coastal and Shelf Science* 171:111–22.

Delandmeter, Philippe, Jonathan Lambrechts, Vincent Legat, Valentin Vallaeys, Jaya Naithani, Wim Thiery, Jean-François Remacle, and Eric Deleersnijder. 2018. 'A Fully Consistent and Conservative Vertically Adaptive Coordinate System for SLIM 3D v0.4 with an Application to the Thermocline Oscillations of Lake Tanganyika'. *Geoscientific Model Development* 11(3):1161–79.

Dissanayake, Awantha, and Atsushi Ishimatsu. 2011. 'Synergistic Effects of Elevated CO2 and Temperature on the Metabolic Scope and Activity in a Shallow-Water Coastal Decapod (Metapenaeus Joyneri; Crustacea: Penaeidae)'. *ICES Journal of Marine Science* 68(6):1147–54. doi: 10.1093/icesjms/fsq188.

Dobbelaere, Thomas, Erinn M. Muller, Lewis J. Gramer, Daniel M. Holstein, and Emmanuel Hanert. 2020. 'Coupled Epidemio-Hydrodynamic Modeling to Understand the Spread of a Deadly Coral Disease in Florida'. *Frontiers in Marine Science* 7.

Duquesne, François, Valentin Vallaeys, Prem Jai Vidaurre, and Emmanuel Hanert. 2021. 'A Coupled Ecohydrodynamic Model to Predict Algal Blooms in Lake Titicaca'. *Ecological Modelling* 440:109418. doi: 10.1016/j.ecolmodel.2020.109418.

ECMWF. 2021. 'Climate Reanalysis | Copernicus'. *Copernicus Climate Change Service*. Retrieved 10 March 2021 (https://climate.copernicus.eu/climate-reanalysis).

Egbert, Gary, and Svetlana Erofeeva. 2002. 'Efficient Inverse Modeling of Barotropic Ocean Tides'. *Journal of Atmospheric and Oceanic Technology* 19(2):183–204.

Émond, Kim, Bernard Sainte-Marie, and Joël Bêty. 2020. 'Long-Term Trends and Drivers of Larval Phenology and Abundance of Dominant Brachyuran Crabs in the Gulf of St. Lawrence (Canada)'. *Fisheries Oceanography* 29(2):185–200. doi: https://doi.org/10.1111/fog.12463.

Epifanio, Charles E., and Jonathan H. Cohen. 2016. 'Behavioral Adaptations in Larvae of Brachyuran Crabs: A Review'. *Journal of Experimental Marine Biology and Ecology* 482:85–105.

Figueiredo, J., C. J. Thomas, Eric Deleersnijder, Jonathan Lambrechts, A. H. Baird, S. R. Connoly, and E. Hanert. 2021. 'Global Warming Weakens Connectivity among Coral Populations'. *Nature Climate Change, in Review.*

Florida Fish And Wildlife Conservation Commission. 2011. '2011 Stone Crab Stock Assessment'. *Florida Fish And Wildlife Conservation Commission*. Retrieved 21 April 2021 (http://myfwc.com/research/saltwater/crustaceans/stone-crabs/stock-assessments/).

Florida Fish And Wildlife Conservation Commission. 2020. 'Stone Crab Season Starts Oct. 15 with Regulation Changes in Place'. *Florida Fish And Wildlife Conservation Commission*. Retrieved 24 May 2021 (http://myfwc.com/news/all-news/stone-crab-1020/).

Frys, Charles, Antoine Saint-Amand, Matthieu Le Hénaff, Joana Figueiredo, Alyson Kuba, Brian Walker, Jonathan Lambrechts, Valentin Vallaeys, David Vincent, and Emmanuel

Hanert. 2020. 'Fine-Scale Coral Connectivity Pathways in the Florida Reef Tract: Implications for Conservation and Restoration'. *Frontiers in Marine Science* 7.

Fujiwara, Masami, Fernando Martinez-Andrade, R. J. David Wells, Mark Fisher, Michaela Pawluk, and Mariah C. Livernois. 2019. 'Climate-Related Factors Cause Changes in the Diversity of Fish and Invertebrates in Subtropical Coast of the Gulf of Mexico'. *Communications Biology* 2(1):1–9.

Gandy, Ryan, Claire Crowley, David Chagaris, and Charles Crawford. 2016. 'The Effect of Temperature on Release Mortality of Declawed <I>Menippe Mercenaria</I> in the Florida Stone Crab Fishery'. *Bulletin of Marine Science* 92(1):1–15.

GBIF Backbone Taxonomy. 2019. 'Menippe Mercenaria (Say, 1818)'. *GBIF Secretariat*. Retrieved 13 March 2021 (https://www.gbif.org/species/5178757).

Gravinese, Philip. 2017. 'Ocean Acidification Impacts the Embryonic Development and Hatching Success of the Florida Stone Crab, Menippe Mercenaria'. *Journal of Experimental Marine Biology and Ecology* 500.

Gravinese, Philip M. 2018. 'Vertical Swimming Behavior in Larvae of the Florida Stone Crab, Menippe Mercenaria'. *Journal of Plankton Research* 40(6):643–54.

Gravinese, Philip M., Ian C. Enochs, Derek P. Manzello, and Robert van Woesik. 2018. 'Warming and PCO2 Effects on Florida Stone Crab Larvae'. *Estuarine, Coastal and Shelf Science* 204:193–201.

Gravinese, Philip M., Ian C. Enochs, Derek P. Manzello, and Robert van Woesik. 2019. 'Ocean Acidification Changes the Vertical Movement of Stone Crab Larvae'. *Biology Letters* 15(12):1–7.

Gräwe, Ulf, and Jörg-Olaf Wolff. 2010. 'Suspended Particulate Matter Dynamics in a Particle Framework'. 10:21–39.

Grech, Alana, Emmanuel Hanert, Len McKenzie, Michael Rasheed, Christopher Thomas, Samantha Tol, Mingzhu Wang, Michelle Waycott, Jolan Wolter, and Rob Coles. 2018. 'Predicting the Cumulative Effect of Multiple Disturbances on Seagrass Connectivity'. *Global Change Biology* 24(7):3093–3104. doi: 10.1111/gcb.14127.

Grech, Alana, Jolan Wolter, Rob Coles, Len McKenzie, Michael Rasheed, Christopher Thomas, Michelle Waycott, and Emmanuel Hanert. 2016. 'Spatial Patterns of Seagrass Dispersal and Settlement'. *Diversity and Distributions* 22(11):1150–62. doi: https://doi.org/10.1111/ddi.12479.

Gulf Shores Marine Fisheries Commission. 2001. *Summary Table of the Stone Crab, *Menippe Mercenaria*,: Life History for the Gulf of Mexico*.

Hamilton, Peter. 1990. 'Deep Currents in the Gulf of Mexico'. *Journal of Physical Oceanography* 20(7):1087–1104.

Haney, Robert L. 1991. 'On the Pressure Gradient Force over Steep Topography in Sigma Coordinate Ocean Models'. *Sigma Coordinate Ocean Models. Journal of Physical Oceanography, (4), 610–619.* 21(4):610–19.

Harper, David. 1992. 'What Is Eutrophication?' Pp. 1–28 in *Eutrophication of Freshwaters*. Dordrecht: Springer Netherlands.

Hastings, Alan, and Louis Botsford. 2003. 'Comparing Designs of Marine Reserves for Fisheries and for Biodiversity'. *Ecological Applications - ECOL APPL* 13:65–70.

He, Ruoying, and Robert H. Weisberg. 2002. 'West Florida Shelf Circulation and Temperature Budgetfor the 1999 Spring Transition'. *Continental Shelf Research* 22:719–48.

He, Ruoying, and Robert H. Weisberg. 2003. 'West Florida Shelf Circulation and Temperature Budget for the 1998 Fall Transition'. *Continental Shelf Research* 23(8):777–800.

Hoegh-Guldberg, O., R. Cai, E. S. Poloczanska, P. G. Brewer, S. Sundby, K. Hilmi, V. J. Fabry, and S. Jung. 2014. 'The Ocean'. Pp. 1655–1731 in. Cambridge, United Kingdom and New York, NY, USA: Cambridge University Press.

INSTAAR, University of Colorado. 2011. 'Seafloor Substrates Griddings, Gulf of Mexico'.

Jones, Geoffrey, Maya Srinivasan, and Glenn Almany. 2007. 'Population Connectivity and Conservation of Marine Biodiversity'. *Oceanography (Washington D.C.)* 20:100–111.

Krimsky, Lisa S., and Charles E. Epifanio. 2008. 'Multiple Cues from Multiple Habitats : Effect of Metamorphosis of the Florida Ston Crab, Menippe Mercenaria'. *Journal of Experimental Marine Biology and Ecology* 358(2):178–84.

Krimsky, Lisa S., Philip M. Gravinese, Richard A. Tankersley, and Charles E. Epifanio. 2009. 'Patterns of Larval Release in the Florida Stone Crab, Menippe Mercenaria'. *Journal of Experimental Marine Biology and Ecology* 373(2):96–101.

Kuffner, Ilsa B., Barbara H. Lidz, J. Harold Hudson, and Jeffrey S. Anderson. 2015. 'A Century of Ocean Warming on Florida Keys Coral Reefs: Historic In Situ Observations'. *Estuaries and Coasts* 38(3):1085–96. doi: 10.1007/s12237-014-9875-5.

Kuhn, Abigail A. 2017. 'Effects of Temperature on Growth and Molting in Blue Crabs Effects of Temperature on Growth and Molting in Blue Crabs (Callinectes Sapidus) and Lesser Blue Crabs ((Callinectes Sapidus) and Lesser Blue Crabs (Callinectes SimilisCallinectes Similis))'. University of Southern Mississippi.

Kurihara, Haruko. 2008. 'Effects of CO2-Driven Ocean Acidification on the Early Developmental Stages of Invertebrates'. *Marine Ecology Progress Series* 373:275–84.

Li, Yanfang, Eric Wolanski, Zhenfei Dai, Jonathan Lambrechts, Cheng Tang, and Hua Zhang. 2018. 'Trapping of Plastics in Semi-Enclosed Seas: Insights from the Bohai Sea, China'. *Marine Pollution Bulletin* 137:509–17.

Lindberg, W. J., and M. J. Marshall. 1984. *Species Profiles: Life Histories and Environmental Requirements of Coastal Fishes and Invertebrates (South Atlantic): Stone Crab.* Washington (D.C.): Florida Gulf Coast University.

Liu, Yonggang, and Robert H. Weisberg. 2012. 'Seasonal Variability on the West Florida Shelf'. *Progress in Oceanography* 104:80–98.

Martínez-López, Benjamín, Jorge Zavala-Hidalgo, and Carlos Gay García. 2014. 'Stochastic Resonance and Anti-Cyclonic Rings in the Gulf of Mexico'. Pp. 253–61 in *Simulation and Modeling Methodologies, Technologies and Applications*, *Advances in Intelligent Systems and Computing*, edited by M. S. Obaidat, J. Filipe, J. Kacprzyk, and N. Pina. Cham: Springer International Publishing.

Metzger, Rebekka, Franz J. Sartoris, Martina Langenbuch, and Hans O. Pörtner. 2007. 'Influence of Elevated CO2 Concentrations on Thermal Tolerance of the Edible Crab Cancer Pagurus'. *Journal of Thermal Biology* 32(3):144–51. doi: 10.1016/j.jtherbio.2007.01.010.

Mieszkowska, N., M. A. Kendall, S. J. Hawkins, R. Leaper, P. Williamson, N. J. Hardman-Mountford, and A. J. Southward. 2006. 'Changes in the Range of Some Common Rocky Shore Species In Britain — A Response To Climate Change?' Pp. 241–51 in *Marine Biodiversity: Patterns and Processes, Assessment, Threats, Management and Conservation*, *Developments in Hydrobiology*, edited by K. Martens, H. Queiroga, M. R. Cunha, A. Cunha, M. H. Moreira, V. Quintino, A. M. Rodrigues, J. Seroôdio, and R. M. Warwick. Dordrecht: Springer Netherlands.

Morey, Steven, Marguerite Koch, Yanyun Liu, and Sang-Ki Lee. 2017. 'Florida's Oceans and Marine Habitats in a Changing Climate'. in *Florida's Climate: Changes, Variations, & Impacts*.

Murphy, James T. 2020. 'Climate Change, Interspecific Competition, and Poleward vs. Depth Distribution Shifts: Spatial Analyses of the Eastern Bering Sea Snow and Tanner Crab (Chionoecetes Opilio and C. Bairdi)'. *Fisheries Research* 223:105417. doi: 10.1016/j.fishres.2019.105417.

National Oceanic and Atmospheric Administration. 2021. 'National Data Buoy Center'. Retrieved 15 October 2020 (https://www.ndbc.noaa.gov/).

NOAA National Geophysical Data Center. 2001. 'U.S. Coastal Relief Model Vol.3 - Florida and East Gulf of Mexico.'

NOAA Ocean Acidification Program. 2020. 'Ocean Acidification Product Suite : The Caribbean Sea and Gulf of Mexico'. *NOAA - Coral Health and Monitoring Program*. Retrieved 20 May 2021 (https://www.coral.noaa.gov/accrete/oaps.html).

North, Elizabeth, Z. Schlag, R. Hood, Ming Li, L. Zhong, Tom Gross, and V. Kennedy. 2008. 'Vertical Swimming Behavior Influences the Dispersal of Simulated Oyster Larvae in a Coupled Particle-Tracking and Hydrodynamic Model of Chesapeake Bay'. *Marine*

Ecology-Progress Series - MAR ECOL-PROGR SER 359:99–115. doi: 10.3354/meps07317.

Nuutila, Esko, and Eljas Soisalon-Soininen. 1994. 'On Finding the Strongly Connected Components in a Directed Graph'. *Information Processing Letters* 49(1):9–14.

Okubo, Akira. 1971. 'Oceanic Diffusion Diagrams'. *Deep Sea Research and Oceanographic Abstracts* 18(8):789–802.

Ong, Kah Sin, and John D. Costlow. 1970. 'The Effect of Salinity and Temperature on the Larval Development of the Stone Crab, Menippe Mercenaria (Say), Reared in the Laboratory'. *Chesapeake Science* 11(1):16–19.

Peliz, Alvaro, Patrick Marchesiello, Jesus Dubert, Martinho Marta-Almeida, Claude Roy, and Henrique Queiroga. 2007. 'A Study of Crab Larvae Dispersal on the Western Iberian Shelf: Physical Processes'. *Journal of Marine Systems* 68(1):215–36.

Pineda, Jesus, Jonathan A. Hare, and Su Sponaugle. 2007. 'Larval Transport and Dispersal in the Coastal Ocean and Consequences for Population Connectivity'. *Oceanography* 20(3):22–39.

Porter, Hugh J. 1960. 'Zoeal Stages of the Stone Crab, Menippe Mercenaria Say'. *Chesapeake Science* 1(3/4):168.

Pörtner, H. O., D. M. Karl, P. W. Boyd, W. W. L. Cheung, S. E. Lluch-Cota, Y. Nojiri, D. N. Schmidt, and P. O. Zaviavlov. 2014. 'Ocean Systems'. Pp. 411–84 in *Climate Change 2014: Impacts, Adaptation, and Vulnerability. Part A: Global and Sectoral Aspects. Contribution of Working Group II to the Fifth Assessment Report of the Intergovernmental Panel on Climate Change*.

Przeslawski, Rachel, Shane Ahyong, Maria Byrne, Gert Wörheide, and Pat Hutchings. 2008. 'Beyond Corals and Fish: The Effects of Climate Change on Noncoral Benthic Invertebrates of Tropical Reefs'. *Global Change Biology* 14(12):2773–95. doi: https://doi.org/10.1111/j.1365-2486.2008.01693.x.

Seyoum, Seifu, Ryan L. Gandy, Claire E. Crowley, and Cecilia Puchulutegui. 2021. 'A Novel Interpretation of Speciation, Hybridization, and Genetic Population Structure of the Stone Crabs Menippe Mercenaria (Say, 1817–1818) and M. Adina Williams & Felder, 1986 (Decapoda: Brachyura: Menippidae)'. *Journal of Crustacean Biology* 41(ruab018). doi: 10.1093/jcbiol/ruab018.

Shanks, Alan L., Brian A. Grantham, and Mark H. Carr. 2003. 'Propagule Dispersal Distance and the Size and Spacing of Marine Reserves'. *Ecological Applications* 13(sp1):159–69. doi: https://doi.org/10.1890/1051-0761(2003)013[0159:PDDATS]2.0.CO;2.

Smagorinsky, J. 1963. 'General Circulation Experiments with the Primitive Equations : I. The Basic Experiment'. *Monthly Weather Review* 91(3):99–164.

Smith, S. D., and E. G. Banke. 1975. 'Variation of the Sea Surface Drag Coefficient with Wind Speed'. *Quarterly Journal of the Royal Meteorological Society* 101(429):665–73.

Sulkin, Stephen D. 1984. 'Behavioral Basis of Depth Regulation in the Larvae of Brachyuran Cra'. *Marine Ecology Progress Series* 15(1/2):181–205.

Sundelöf, Andreas, and Per R. Jonsson. 2012. 'Larval Dispersal and Vertical Migration Behaviour – a Simulation Study for Short Dispersal Times'. *Marine Ecology* 33(2):183–93. doi: https://doi.org/10.1111/j.1439-0485.2011.00485.x.

Tarjan, Robert. 1972. 'Depth-First Search and Linear Graph Algorithms'. *SIAM Journal on Computing* 1(2):146–60.

Thomas, Christopher J., Jonathan Lambrechts, Eric Wolanski, Vincent A. Traag, Vincent D. Blondel, Eric Deleersnijder, and Emmanuel Hanert. 2014. 'Numerical Modelling and Graph Theory Tools to Study Ecological Connectivity in the Great Barrier Reef'. *Ecological Modelling* 272:160–74. doi: 10.1016/j.ecolmodel.2013.10.002.

Turner, R. E., and N. N. Rabalais. 2019. 'The Gulf of Mexico'. Pp. 445–64 in *World Seas: An Environmental Evaluation - Volume I: Europe, the Americas and West Africa*.

U.S. Census Bureau. 2020. 'Resident Population in Alabame, Louisiana, Mississippi, Texas and Florida'. *FRED Graph*. Retrieved 24 November 2020 (https://fred.stlouisfed.org/graph/?id=ALPOP,LAPOP,MSPOP,TXPOP,FLPOP,).

Vallaeys, Valentin, Tuomas Kärnä, Philippe Delandmeter, Jonathan Lambrechts, António M. Baptista, Eric Deleersnijder, and Emmanuel Hanert. 2018. 'Discontinuous Galerkin Modeling of the Columbia River's Coupled Estuary-Plume Dynamics'. *Ocean Modelling* 124:111–24.

Vukovich, Fred M., Bobby W. Crissman, Mark Bushnell, and William J. King. 1979. 'Some Aspects of the Oceanography of the Gulf of Mexico Using Satellite and in Situ Data'. *Journal of Geophysical Research* 84(C12):7749.

Wallace, Ryan B., Hannes Baumann, Jason S. Grear, Robert C. Aller, and Christopher J. Gobler. 2014. 'Coastal Ocean Acidification: The Other Eutrophication Problem'. *Estuarine, Coastal and Shelf Science* 148:1–13.

Weisberg, Robert H., Zhenjiang Li, and Frank Muller-Karger. 2001. 'West Florida Shelf Response to Local Wind Forcing: April 1998'. *Journal of Geophysical Research: Oceans* 106(C12):31239–62.

Yoskowitz, David, Leon Cuauhtemoc, James Gibeaut, Brach Lupher, Mayra Lopez, Gail Sutton, Carlotta Santos, and Larry McKinney. 2013. *Gulf 360: State of the Gulf of Mexico*. Texas: arte Research Institute for Gulf of Mexico Studies Texas A&M University-Corpus Christi.

Young, A. M., and T. L. Hazlett. 1978. 'The Effect of Salinity and Temperature on the Larval Development of Clibanarius Vittatus (Bosc) (Crustacea: Decapoda: Diogenidae)'. *Journal of Experimental Marine Biology and Ecology* 34(2):131–41.

Zavala-Hidalgo, Jorge, Rosario Romero-Centeno, Adriana Mateos-Jasso, Steven L. Morey, and Benjamín Martínez-López. 2014. 'The Response of the Gulf of Mexico to Wind and Heat Flux Forcing: What Has Been Learned in Recent Years?' *Atmósfera* 27(3):317–34.

Zhang, Jia-Zhong, and Charles J. Fischer. 2014. 'Carbon Dynamics of Florida Bay: Spatiotemporal Patterns and Biological Control'. *Environmental Science & Technology* 48(16):9161–69.

Evaluation of the impacts of climate change on the distribution of Florida stone crab larvae on the West Florida Shelf

Lauranne Alaerts

Ocean acidification and ocean warming are the two components of climate change that impacts marine life the most. The commercially important Florida stone crab, *Menippe mercenaria*, is one of the species that is going to be affected by those changes. In this study we investigated the impacts of climate change on the distribution of the stone crab larvae on the West Florida Shelf. To understand the dispersion of the larvae, we coupled SLIM3D, a multi-scale ocean model, with a larval dispersal model. We then conducted a connectivity study and evaluated the impacts of climate change analyzing three different scenarios, one presenting the dispersion of the larvae for present conditions and the two others presenting the dispersion for mild and extreme climate change. The results show a clear impact of climate change on larval dispersal and on the subsequent crabs distribution. In the future, climate change could result in stone crabs moving north or to deeper waters. The second impact would be the increase in the number of larvae settling in the non-fishing zone, where the water depth exceeds 30 m. The distance traveled by larvae is going to decrease, resulting in an increase of self-recruitment and decrease of the size of sub-populations. The last impact we identified is the possibility of a shift of the spawning period earlier in the season. We also evaluated that the habitats in the non-fishing zone cannot serve as a significant source of larvae for the habitats in the fishing zone since there is very little exchange between the two zones. Overall, this work could help local authorities to better understand *M. mercenaria* and to take actions regarding the fishery management and its future considering the upcoming changes in the ocean conditions.

UNIVERSITÉ CATHOLIQUE DE LOUVAIN
Faculté des bioingénieurs
Croix du Sud, 2 bte L7.05.01, 1348 Louvain-la-Neuve, Belgique | **www.uclouvain.be/agro**